UNIVERSIDADE D
COIMBRA

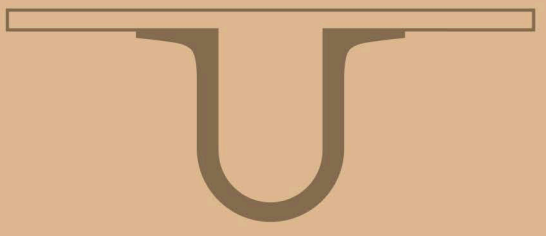

Marina Duarte de Macedo Oliveira

Mathematical Model for the Growth of Glioblastoma

Thesis submitted to the
University of Coimbra for the degree of
Master in Biomedical Engineering

September 2018

• U  C •

FCTUC FACULDADE DE CIÊNCIAS
E TECNOLOGIA
UNIVERSIDADE DE COIMBRA

Marina Duarte de Macedo Oliveira

Mathematical Model for the Growth of Glioblastoma

Thesis submitted to the
University of Coimbra for the degree of
Master in Biomedical Engineering

Supervisors:
Prof. Dr. Rui Travasso (CFisUC)
Prof. Dr. João Carvalho (CFisUC)

Coimbra, 2018

Acknowledgments

First of all, I would like to thank both my advisors for offering me the unique opportunity to work in a project I always wanted to develop. Although the initial phase was troubled and I did not know exactly how to tackle the problem proposed, they were relentless.

Throughout this year, mainly in the second semester, exclusively dedicated to the development of the thesis, several difficulties were crossed from the initial understanding of the base model to the phase of the choice of the approach to be used to simulate this system. In addition, I came across the difficulty of developing a program in a language I had never worked with before. However, I have been able to understand the level of frustration that needs to be overcome when implementing something like this and how this frustration is essential to the learning process. Therefore, I would also like to thank my family and all my friends for their constant patience and support in the most troubled days.

Resumo

Os tumores cerebrais astrocíticos, incluíndo os glioblastomas, são neoplasias incuráveis, caracterizadas pelo crescimento intrusivo difuso. Os astrocitomas são capazes de estender protrusões membranares ultra-longas designadas microtubos tumorais. Utilizam-nas como vias de invasão, proliferação e interconexão do cérebro a longas distâncias. A rede resultante permite a comunicação multicelular através de *gap junctions*. Quando ocorrem danos celulares a este tumor, os microtubos tumorais são cruciais para a reparação da rede, não servindo apenas como via de transmissão de moléculas químicas, mas também de organelos. A desconexão de células de um astrocitoma, tendo como alvos seus microtubos tumorais, surge como um novo princípio para a redução da resistência aos tratamentos convencionais. Este projeto envolve o desenvolvimento de um modelo computacional, a exploração de vários parâmetros de modo a simular o crescimento, a interação entre as células de um glioblastoma e sua interação com os vasos sanguíneos. O modelo é inspirado no modelo de *phase field* para o crescimento de novos vasos sanguíneos. A dinâmica da interface entre os capilares, as células e o estroma é tratada com o formalismo do modelo de *phase field*. A ativação do fenótipo de tip cell nas células endoteliais é implementada no modelo através de agentes. A mesma abordagem é usada para a ponta dos microtubos tumorais. Os vasos seguem o gradiente de um fator efetivo, neste caso o fator de crescimento endotelial vascular (VEGF), e os microtubos das células de glioma seguem o gradiente de outro fator efetivo, que assumimos ser o fator de crescimento tumoral, também chamado fator de crescimento transformador (TGF).

Abstract

Astrocytic brain tumours, including glioblastomas, are incurable neoplasms characterized by diffusely infiltrative growth. Astrocytomas extend ultra-long membrane protrusions called tumour microtubes and use them as routes for brain invasion, proliferation and interconnection over long distances. The resulting network allows multicellular communication through gap junctions. When damage occurs, the tumour microtubes are crucial for the repair of the network since they are not only a route for molecules but also for organelles. Disconnection of astrocytoma cells by targeting their tumour microtubes emerges as a new principle to reduce the resistance of this disease to conventional treatments. This project involves the development of a computational model and a exploration of the various parameters in order to simulate the growth and the interaction between the cells of a glioblastoma and its interaction with the blood vessels, draw quantitative conclusions about the mechanisms of movement and communication within a glioblastoma and find suggestions for new therapeutic targets to regulate the growth of these tumours. The model is inspired by a phase-field model for the growth of new blood vessels. The dynamics of the interface between the capillaries, the cells and the stroma, is treated with a phase-field model formalism. The activation of the tip cell phenotype in endothelial cells is implemented in the model through an agent-based component. The same approach is used for the tip of the tumour microtubes. The vessels follow the gradient of an effective factor, in this case the vascular endothelial growth factor (VEGF), and the microtubes of the glioma cells follow the gradient of another effective factor, that we will assume to be tumour growth factor, also called transforming growth factor (TGF).

Acronyms

VEGF Vascular Endothelial Growth Factor
TGF Tumour Growth Factor
CSF Cerebrospinal fluid
BBB Blood-brain barrier
CNS Central Nervous System
PNS Peripheral Nervous System
GBM Glioblastoma Multiforme
TERT Telomerase Reverse Transcriptase
MGMT O-6-methylguanine-DNA methyltransferase
IDH Isocitrate Deshydrogenase
ZEB1 Zinc Finger E-box binding homeobox 1
TNTs Tunneling Nanotubes
mTOR Mammalian Target of Rapamycin
IP3 Inositol Triphosphate
Cx43 Connexin 43
TMs Tumour Microtubes
MPLSM Multi-photon Laser Scanning Microscopy
MIPs Maximum intensity Projections
GBMSCs Glioblastoma-Derived Mesenchymal Stem Cell
ICMs Intracellular Calcium Waves
GFP Green Fluorescent Protein
RFP Red Fluorescent Protein
GAP-43 Growth associated protein 43
ETC Endothelial tip cell
EC Endothelial cell
ECM Extracellular matrix
Dll4 Delta-like 4
CAs Cellular Automata

List of Figures

List of Tables

Contents

1

Biological Introduction

1.1 Glioma Classification

Gliomas comprise about 80 per cent of all malignant brain tumours and kill patients within 1 year of diagnosis. This type of tumour originates from the glial cells of the brain or the spine. [5, 6] They can be categorized: 1) by cell type; 2) by grade and 3) by location. In terms of cell type, gliomas are named not necessarily according to which type of cell they originate from, but rather from the type of cell they share the higher number of histological features, as shown in Table 1.1. [7]

Ependymomas are developed from or share features with ependymal cells which are the glial cells that compose the neuroepithelial cell lining of the ventricular system localized in the brain and in the central canal of the spinal cord. These cells are responsible for neuroregeneration processes and for the production of cerebral spinal fluid (CSF). Ependymal cells have a cuboidal to columnar structure and have cilia microvilli on the surfaces to enable the absortion and circulation of the CSF.

Astrocytomas are developed from or share features with astrocytes which are star-shaped glial cells present in the brain and the spinal cord. They play several active roles in the brain. The most important ones are the the secretion and/or reuptake of neural transmitters and the maintenance of the blood–brain barrier (BBB). [8]

Oligodendrogliomas are developed from or share features with oligodendrocytes. Oligodendrocytes are glial cells responsible for supporting and insulating neurons by creating the myelin sheath for their axons in the central nervous system (CNS). This function is the equivalent to the the one performed by Schwann cells in the peripheral nervous system (PNS). [9]

Brainstem gliomas are developed from glial cells in the brainstem which has three parts, the pons, that controls critical functions such as breathing, which makes surgery extremely dangerous, the midbrain, and medulla. [7]

The optic nerve glioma is developed in or around the optic nerve, also known as cranial nerve II. This is a paired nerve that is responsible for the transmission of visual information from the retina to the brain. Contrary to popular belief, this nerve is part of the CNS rather than the PNS, since it is derived from the diencephalon (optic stalks) during embryonic development. [**?**]

Table 1.1: Classification of Gliomas by Type of Cell

Ependymomas	Astrocytomas	Oligodendrogliomas	Brainstem glioma	Optic nerve glioma
Developed from or shares features with ependymal cells	Developed from or shares features with astrocytes	Developed from or shares features with oligodendrocytes	Developed in the brainstem	Developed in or around the optic nerve

In terms of grade, gliomas are classified by its pathological impact and diagnostics. This is determined according to WHO Classification of Tumours of the Central Nervous System, as shown in Table 1.2. Hence, tumours are graded from I, meaning the least advanced disease and the best prognosis, to IV, which are the most advanced disease and the ones that have worst prognosis.

Table 1.2: Classification of Gliomas by Grade

Low-grade [WHO grade I-II]	High-grade [WHO grade III–IV]
Well-differentiated (not anaplastic) with benign tendencies, a uniform rate of recurrence and increase in grade over time.	Undifferentiated or anaplastic and carry a worse prognosis.

In terms of location, gliomas are classified according to whether they are above or below the tentorium, which is a brain membrane that separates the cerebrum from the cerebellum. [7]

Table 1.3: Classification of Gliomas by Location

Supratentorial	Infratentorial	Pontine
Above the tentorium, in the cerebrum, and mostly found in adults	Below the tentorium, in the cerebellum, and mostly found in children	Located in the pons of the brainstem.

The major obstacle to finding a cure for these type of tumours is its diffusive invasion pattern, since the glioma escapes a complete surgical resection. [10] The diffuse low-grade and intermediate-grade gliomas have a highly variable and unpredictable behavior. Some of them quickly progress to a glioblastoma, also known as glioblastoma multiforme (GBM). Its exact cellular origin of is uncertain: it is thought that a glioblastoma originates from several types of glial cells, such as astrocytes and oligodendrocyte progenitor cells and neural stem cells. [11]

Gliomas can be genomically characterized by one or more mutations, such as mutations in the telomerase reverse transcriptase (TERT) promoter, mutations in isocitrate dehydrogenase (IDH) gene, and the codeletion of chromosome arms 1p and 19q. [12] They can also be epigenomically characterized based on the methylation of the O-6-methylguanine-DNA methyltransferase (MGMT) gene. [13] These molecular differences are associated with different survival rates, as shown in Figure 1.1.

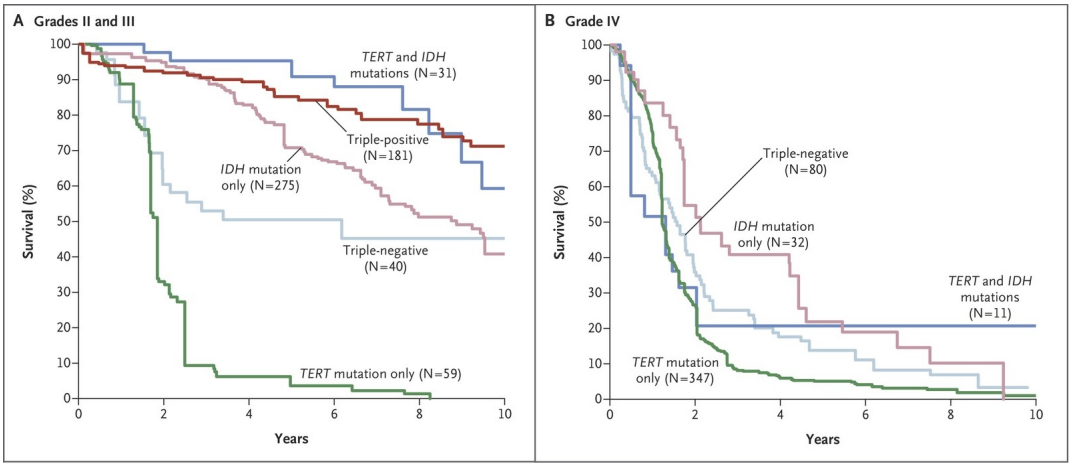

Figure 1.1: Adjusted Kaplan–Meier Estimates of Overall Survival in the Glioma Molecular Groups. [1]

1.1.1 Molecular Features

In terms of molecular features, it is important to mention the zinc finger E-box binding homeobox 1 (ZEB1) transcription factor. This transcription factor is preferentially expressed in the invasive glioma cells. Its expression is associated with the prediction of shorter survival and of poor Temozolomide response. Temozolomide is an alkylating agent that is used in the treatment of astrocytoma and GBM. Hence, ZEB1 is an important molecule for glioma recurrence, a marker of tumour cells capable of invading and a potential therapeutic target.[14]

Both astrocitomas and oligodendrogliomas have the IDH mutation. [11] However, the oligodendroglioma is less invasive and far more vulnerable. [15, 16] The codeletion of the chromosomal parts 1p and 19q that characterizes oligodendrogliomas but is absent in the case of astrocytomas, and it is associated with the lower vulnerability of the latter to radio and chemotherapy, hence the lower survival rate. The specific mechanism responsible for this resistance encoded in the 1p/19q intact astrocytomas remains to be clarified. [2]

1.2 Cellular Communication

Cellular communication mechanisms, including chemical synapses, gap junctions, and plasmodesmata are known to be crucial for the development and maintenance of multicellular organisms. More recently, it was described the formation of nanotubular structures between cells that are rich in actin and create complex networks like the cytonemes characterized in Drosophila. [17] Drosophila male germline stem cells have the ability to form microtubule based nanotubes. [18]

1.2.1 Cytonemes and Tunnelling Nanotubes

Cytonemes are an attribute of both invertebrate and vertebrate cells, such as mouse limb bud cells. In the case of vertabrate cells they are called tunnelling nanotubes (TNTs). [19] Their exact functionality in tumour biology remains unresolved but their identification, despite being limited

to cell lines, is very well described with the use of immunofluorescent staining. These are long, non-adherent F-actin-based protrusions which connect cells and facilitate intercellular trafficking that were first detected in mesothelioma cell lines and primary human mesothelioma cells. It is now possible to stimulate the TNTs formation and its bidirectional trafficking of vesicles, proteins, and mitochondria, using a specific low serum, hyperglycemic and acidic growth medium. It is also shown that metformin, mammalian target of rapamycin (mTor) inhibitor and everolimus, can effectively suppress the TNTs formation. This structures are now thought to play a crucial role in cancer cell pathogenesis and invasion. [2, 17]

These TNTs are also formed when T-cells make contact, providing a route for HIV-1 transmission. These structures allow calcium-mediated signalling mechanisms between connected myeloid cells. However, in the case of a T-cell this dynamic junction that is formed persists. [20]

Hence, TNTs are protrusions that reach lengths of tens of microns and diameters of hundred of nanometres. These structures are crucial for mediating the signalling of intercellular Ca^{2+}. Spontaneous and inositol trisphosphate (IP3)-evoked Ca^{2+} signals can remain localized or can be propagated along the network as saltatory waves. Immunostaining assays show the presence of endoplasmic reticulum and IP3 receptors along the membrane protrusions. The IP3 receptors propagate the intercellular Ca^{2+} signals along TNTs by inducing the release of Ca^{2+} ions. Therefore, TNTs amplify the Ca^{2+} signals to overcome the passive diffusion limitations, resembling a chemical analog of the transmission of action potentials. [21]

TNTs mediate the bidirectional flow of signals between TNT-connected cells over distances of 10 to 70 μm. The strength of the coupling depends on the length and number of TNT connections. Gap junctions also have an important role: connexin 43 (Cx43) immunoreactivity is frequently detected in TNTs, and the coupling is voltage-sensitive. The cell types with no connexin 43 does not show TNT-dependent coupling. Hence, TNT-mediated signals are transmitted through gap junctions between the TNT and the cell. [**?**]

1.2.1.1 Tumour Microtubes

It has been shown that there is a physical connection between the glioma cells with relevance for tumour function and resistance. These structures are called tumour microtubes (TMs) and are conceptually and physically similar to cytonemes and TNTs, but wider, capable of reaching several micrometers. They are important for the spread of chemical particles, stem cell signalling and functional cell-cell coupling. Additionally, these structures are responsible for facilitating the selective transfer proteins, organelles, membrane vesicles and large molecules. Interestingly they seem to block the flow of small molecules. [2, 22]

These protrusions infiltrate the brain as shown in Figure 1.2. Its protrusion tips are highly dynamic and similar to the neuronal growth cones of the neurons. With tumour progression, the number of cellular protrusions increases greatly and the TMs are able to reach 500 micrometers in length. [2]

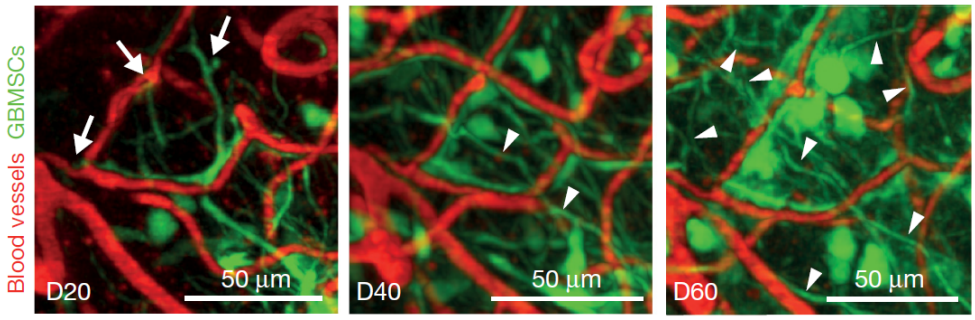

Figure 1.2: In vivo Multiphoton Laser Scanning Microscopy (MPLSM) maximum intensity projections (MIPs) of glioblastoma cell lines (GBMSCs) growing in the mouse brain over 60 days. Arrows indicate thin cellular protrusions extending into the normal brain and arrowheads indicate the long intratumoral protrusions. [2]

Represented in figure 1.3 are different primary GBMSCs growing to astrocytic tumours in the mouse brain with the formation of TMs.

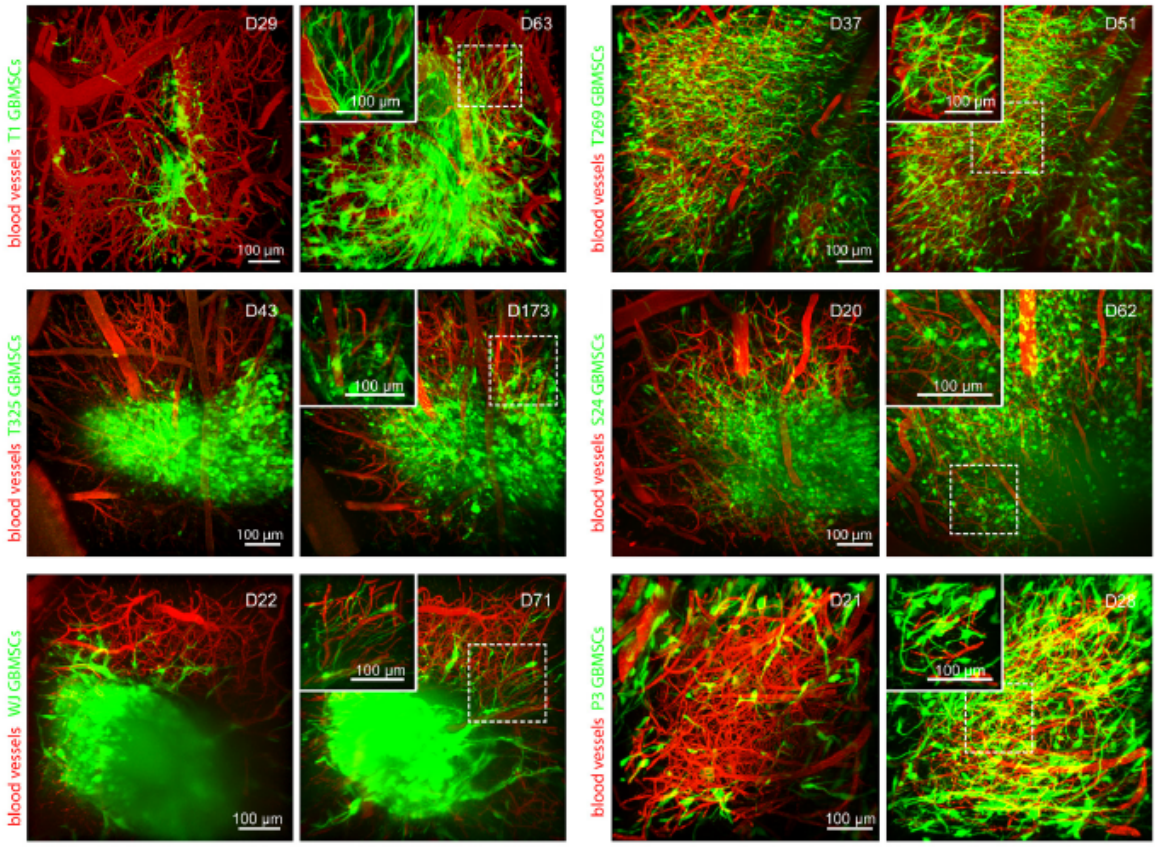

Figure 1.3: In vivo 3D microscopy of 6 different GBMSCs (all noncodeleted for 1p/19q, and IDH wild-type) reveals abundant formation of ultra-long membrane protrusions in the mouse brain. [2]

TMs are actin-rich and are enclosed by a continuous cell membrane, as shown in Figure 1.4. These features are also typical in the TNTs and cytonemes described previously. These new type of membrane tubes have a unique composition and a very potent motility machinery with

more dynamic thin membrane tubes originating from the more stable and thicker ones. The cell membrane enclosed tubes contain mitochondria and microvesicles, which indicates the capacity for local ATP production and vesicle trafficking. [2]

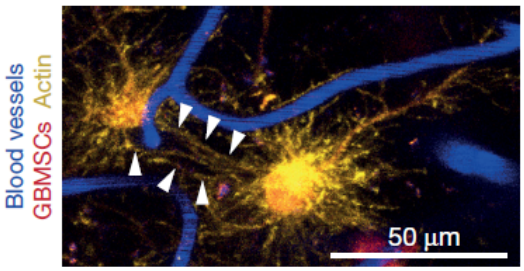

Figure 1.4: In vivo MPLSM images of the actin-rich protrusions that perform the connection between single tumour cells. [2]

As one can see in Figure 1.5, the 3D rendering of the in vivo imaging of membrane tube development over time, reveals links that create a multicellular anatomical network. The tubes can be a result of cell division, with stable contact of daughter cells over long distances or a result of linkage of distant tumour cells.

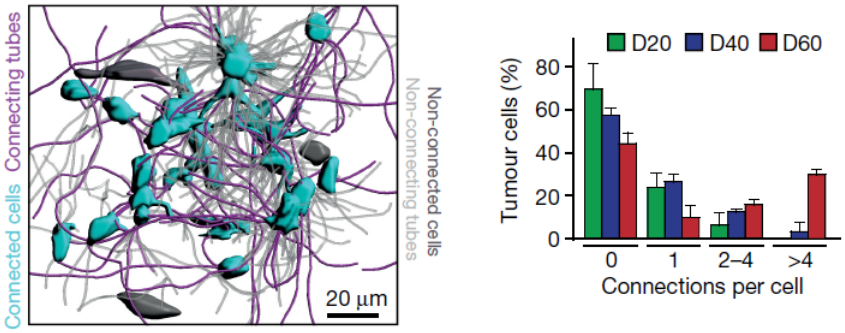

Figure 1.5: The image on the left is a 3D rendering (z dimension 90 micrometers) of membrane microtubes interconnecting the single cells of the GBMSCs. The graph on the right represents the number of TMs per tumour cell that connect each cell to another tumour cell (n = 141–437 cells in n = 3 mice). Both images are in vivo MPLSM. [2]

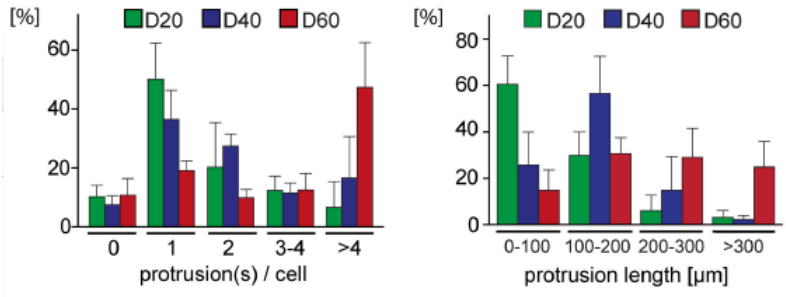

Figure 1.6: These graphs show the characterization of membrane microtubes in astrocytoma mouse models by demonstration the number and length of protrusions during tumour progression. [2]

These discovered TMs are ultra-long, long-lived, and thicker membrane extensions that are shown in images 1.2 and 1.3, and are a new type of cell structure. Their high content of F-actin resembles the TNTs already described. However, the TNTs have a width of below 1 micrometer, a length of tens of micrometers and a life span of less than 60 minutes. Shown in Figures 1.6 and 1.7, are the TMs that characterize human astrocytomas. [2]

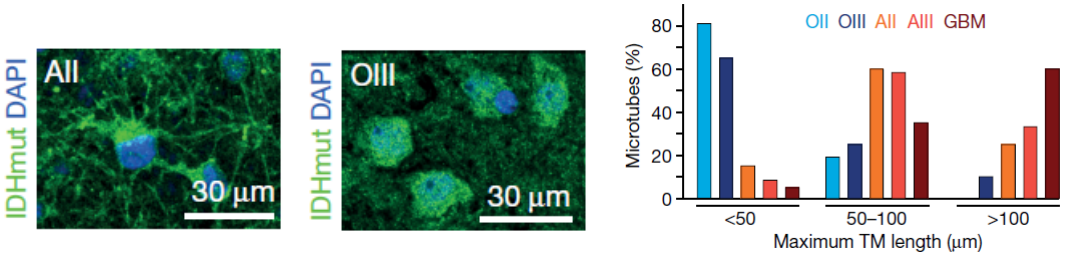

Figure 1.7: The two images on the left is a representative confocal IDH mutation-specific immunofluorescence images of a human astrocytoma grade II and the image on the right is the case for an oligodendroglioma grade III. Both images are in vivo MPLSM. The Graph on the right demonstrates the maximum length of IDH positive microtubular structures in human oligodendrogliomas (1p/19q codeleted) grade II and III and astrocytomas (1p/19q non-codeleted) grade II, III and grade IV GBM (n = 20–24 patients per tumour entity, n = 105 total). Error bars show s.d.[2]

1.2.2 Physical Comunication: Transport of Organelles

The TMs, as shown in Figure 1.3, are used as tracks for the travelling of cell organelles, in this case, the nuclei after mitosis. This type of TMs formation is a novel means of tumour dissemination.[2]

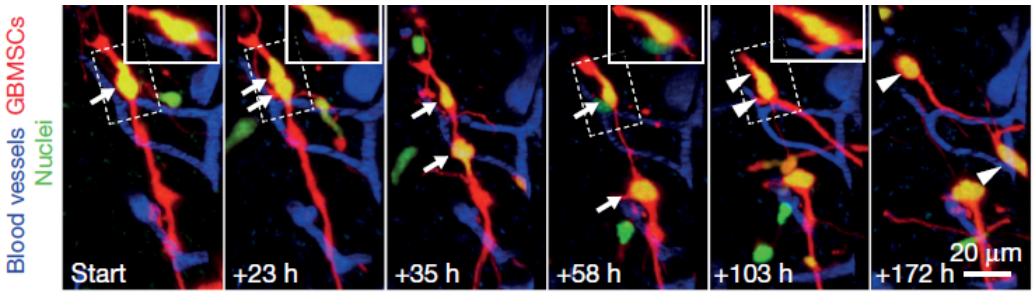

Figure 1.8: In vivo MPLSM 3D images of the nuclei travelling along the cellular protrusions of S24 GBMSCs, after nuclear division (at 23 and 103 h). [2]

1.2.3 Chemical Communication: Intercellular Calcium Waves

Intercellular calcium waves (ICWs) are grouped into cell activity cells in multicellular networks, including astrocytes, neurons, and radial glial cells during the development of the central nervous system. These ICWs travel through the TMs, as represented in Figure 1.9. [23, 24, 25, 26]

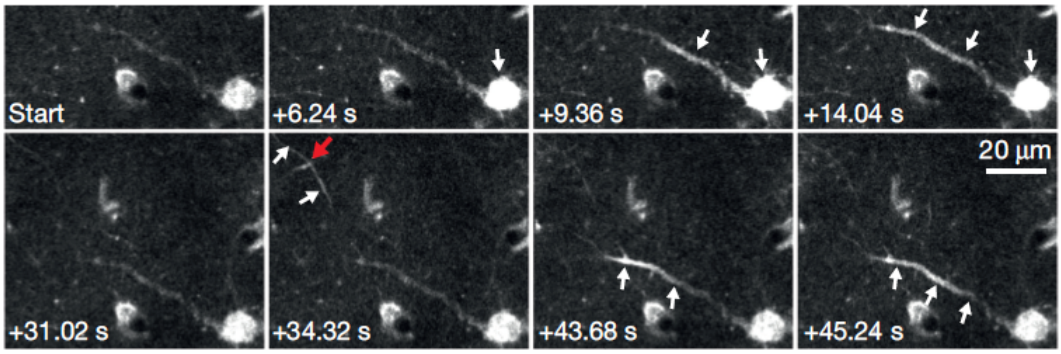

Figure 1.9: Time-lapse image of travelling ICWs along TMs of GBMSCs. Red arrow shows the crossing of two TMs, with simultaneous calcium peak.[2]

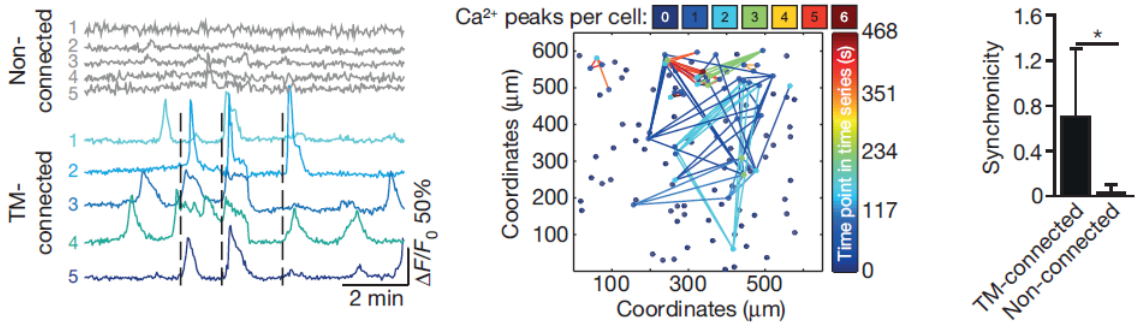

Figure 1.10: The image on the left represents the calcium transients of TM-connected cells in blue and the calcium transients non-connected GMBSCs in grey. The broken lines mark the synchronous calcium transients. The middle image is a representative heat map of calcium transients between GBMSCs. The image on the right represents the synchronicity of calcium peaks in GBMSCs, shown for the TM-connected versus the non-TM-connected tumour cells. [2]

1.2.4 Network Repair

The TM-connected astrocytoma cell networks are capable of repairing themselves, and resist radiotherapy. These tumour cells are able to detect when one cell is damaged, they extend the TMs in order to establish a physical contact, divide their nucleus and send it along the tube, regenerating the designated cell. This process can be seen in Figure 1.11 and 1.12.

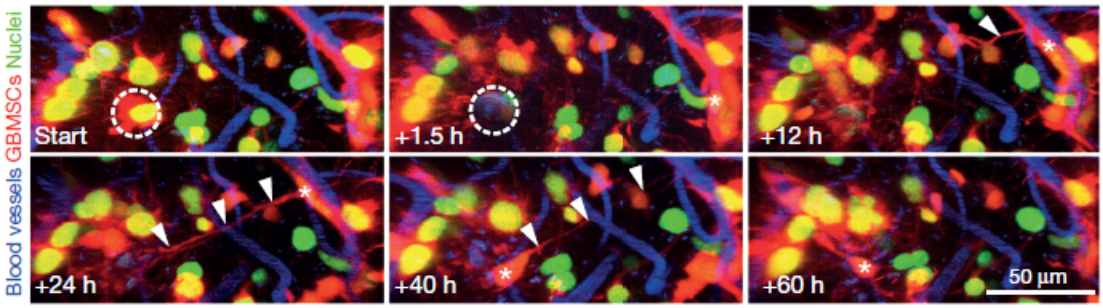

Figure 1.11: Ttime series of a tumour region after laser-induced killing of a GMBSC, shown with a dashed circle. Over time a TM, shown in arrowheads, is extended, and a nucleus, marked with an asterisk, that is translocated via that TM to the place the killed cell had been located. [2]

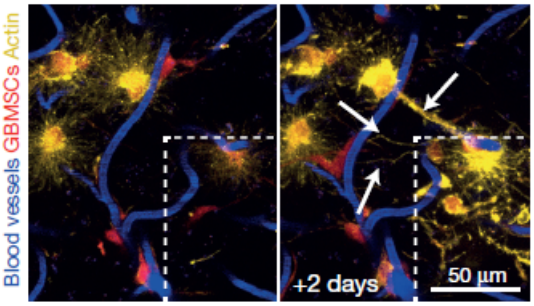

Figure 1.12: Time course after laser-induced photodamage (dotted area). The arrows point to the GBMSC TMs extending into the photodamaged region. [2]

1.2.5 Origin of TM formation

The origin of the TM-connections between astrocytoma cells, and long-time tracking of TM-extending cells is not well understood. Figure 1.13 illustrates the two hypothesis for their origin. In hypothesis 1, the tumour cells remain connected after cell division with their ancestors. In this case, only connections between cells of the same colour would be expected: green, given by green fluorescent protein (GFP) or red, given by red fluorescent protein (RFP). In hypothesis 2, the tumour cells only connect to unrelated glioma cells. Here, 50% of the connections would be between cells of different colour (GFP–RFP or RFP–GFP that appear grey), and 25% of the same colour. The results showed that both mechanisms can be present.

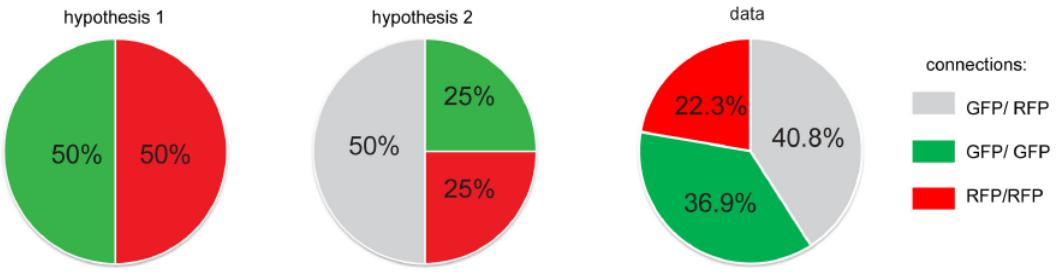

Figure 1.13: Graphs illustrating two theoretically possible ways of intercellular connections by membrane tubes in a model of two tumour cell populations marked with 2 different fluorescent proteins. In the real data set, where a 1:1 mixture of either GFP or RFP expressing GBMSCs was co-injected into the mouse brain, revealing that both potential mechanisms are in place (n = 164 connections in n = 3 mice). [2]

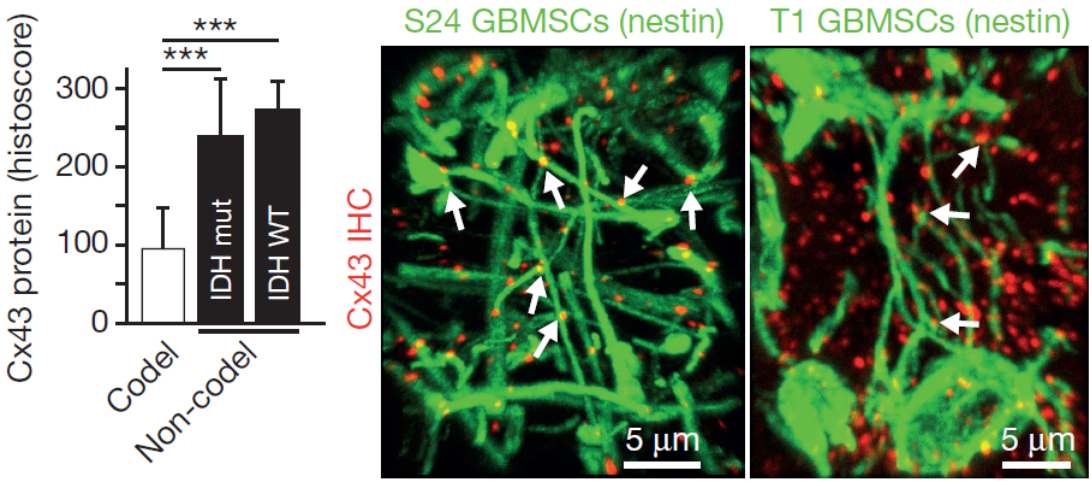

Figure 1.14: The image on the left represents the quantification of Cx43 protein expression detected by immunohistochemistry in the 1p/19 non-codeleted (IDH wild-type and IDH mutated) versus the codeleted human gliomas. The two images on the right represent Nestin and Cx43 double-immunofluorescence in GBMSC tumours. It reveals punctate Cx43 immunoreactivity particularly at the TMs of the astrocytoma cells, frequently located at the place where two different TMs crossed each other.[2]

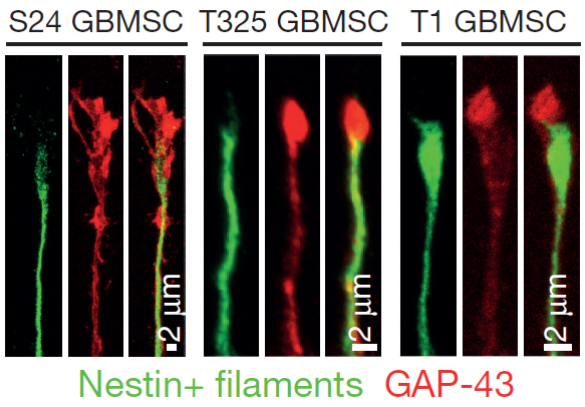

Figure 1.15: Immunocytological images of growth associated protein 43 (GAP-43), with preferential GAP-43 localization at the tip of TMs. [2]

The mechanism of interconnection of tumour cells through ultra-long and highly functional TMs is of great importance for the progression and tumour resistance of astrocytomas and depends greatly on the molecular pathways that are active when there is no 1p/19q codeletion. The multicellular network maintains communication through the Cx43 slot junction connections, which are also highly expressed in non-malignant astrocytes, being responsible for their connection in cellular networks, as one can see in Figure 1.14. It is thought that the possible mechanism for this resistance is the maintenance of calcium homoeostasis throughout the network. Increases in intracellular calcium levels are required for the induction of cytotoxicity and apoptotic cell death in glioma cells. Thus, TMs can serve as a critical distribution pathway for small molecules, such as calcium, to achieve non-lethal levels.

TMs, which are generated by high GAP-43 cell expression, as well as in the growth cones of neurons, as can be seen in figure 1.15, allow for efficient tumour progression, cellular network communication and high resistance. The importance of the TMs in brain tumour progression is illustrated in Figure 1.16. Thus, pharmacological targeting for the formation and maintenance of TMs is a potential therapeutic pathway for combating conventional treatment-resistant brain tumours.

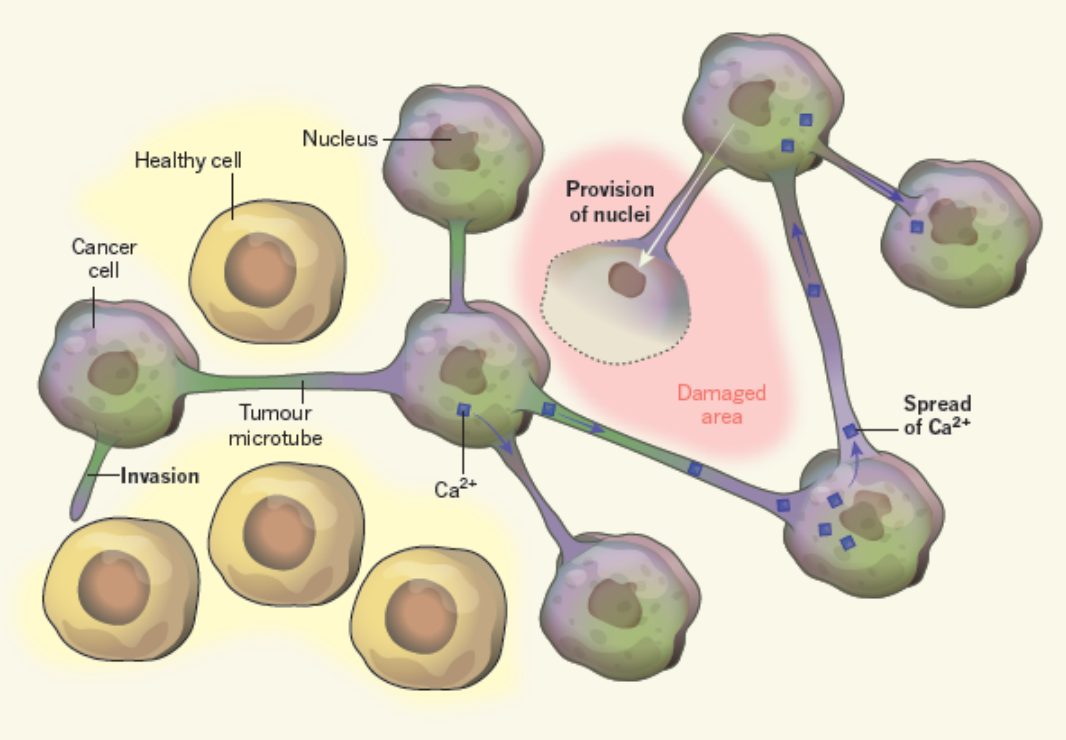

Figure 1.16: Schematic illustration of the role of TMs in brain tumour progression with anatomical and molecular mechanisms for tumour dissemination and network function.[2]

The effective factor responsible for driving the TMs remains to be resolved. For this work, it will be assumed that TGF is effective factor.

1.3 Angiogenesis

The cardiovascular system provides transport for the functional requirements of the organisms. Thus, it delivers not only oxygen but also nutrients to the cells of other tissues, providing them with the necessary conditions to their metabolic activities. The first morphogenetic process of vascular development is vasculogenesis and occurs exclusively during the early embryonic phase. This process starts with the differentiation of angioblasts, the percursors of the endothelial cells recruited directly from the bone marrow, that ultimatly compose the blood vessels. The angioblasts merge to form a primitive vascular network of small capillaries. Later, the network is remodeled. Then more capillaries are able to sprout from this existing vasculature through a process named angiogenesis with cells such as pericytes and smooth muscle cells cover the endothelial cell walls,

conferring stability to the structure and thus creating a mature vascular network. [27, 28, 29] Blood flow is able to influence the diameter of the vessels leading to an hierarchical network.

In adulthood, most blood vessels remain inert, but due to angiogenesis, they can rapidly be activated in response to certain physiological stimuli, such as those resulting from a state of hypoxia. When media oxygenation is not sufficient, stimuli from media in hypoxia activates pro-angiogenic factors and inhibits anti-angiogenic factors, leading to vascular growth. The opposite happens in the process of vessel regression, where the activated factors are the anti-angiogenic and the inhibited one are the pro-angiogenic. [30, 31]

1.3.1 Tumour Angiogenesis

Under certain conditions such as cancer, new blood vessels nourish diseased tissues and allow tumour cells to escape into the circulation, invading other healthy organs, in a process called metastisation. The supply of nutrients and oxygen, in the case of tumours, is highly inefficient compared to healthy tissues, due to the structural disorganization of the blood vessels that irrigate it. The new vessels formed under these conditions tend to be more fragile, usually without smooth muscle cells, presenting themselves prone to rupture and a complicated remodelling process, compromising circulation. Under these conditions, the medical treatments are usually therapies designed to stop the growth of these small vessels. [27, 28]

1.3.2 Sprouting and Intussusceptive Angiogenesis

There are two types of angiogenic processes. Both cases result in the development of new blood vessels but are characterized by very different morphological events.

Intussusceptive angiogenesis or splitting angiogenesis involves the formation of new blood vessels by a process called protrusion. In this process, a few elements form endothelial bridges towards the lumen and when two of these structures meet, they unite, forming a pillar inside the vessel. This pillar separates the flow and it goes in the longitudinal direction, dividing the vessel in two. This type of angiogenic process is the fastest and most efficient one, because it is not dependent on the rate of endothelial proliferation nor on cell migration. For this reason, this type of angiogenesis plays a key role in the embryonic vascular development where growth is rapid and the resources are limited.

On the other hand, sprouting angiogenesis is the burst of new blood vessels from already existing ones through the motion of tip cells, the leaders, and stalk cells, the followers. The deregulation of sprouting angiogenesis occurrence has been linked to many pathologies. Angiogenesis common among tumour conditions or poorly perfused tissues. The lack of oxygen leads to the secretion of factors that induce endothelial growth. Thus, angiogenesis is considered one of the hallmarks of cancer.

The most common example of a pro-angiogenic factor is VEGF. VEGF induces the expression of anti-apoptotic proteins and inhibits the action of apoptotic proteins on endothelial cells. This substance induces a rapid increase in permeability, activating vascular endothelial tip cell (ETC) phenotype in endothelial cells (EC). In addition, this factor is responsible for promoting the migration of the ETCs towards their gradient and boosting their proliferation.

VEGF finds a capillary vessel, stimulates the endothelial wall and activates them by giving them the acquisition of the tip cell phenotype. In this phenotype the cells are the conducting cells of the new vessel towards an increase in the concentration of angiogenic factors. At the same time, stalk cells, use their great proliferative capacity to follow the development of the vessel.

The tip cells have long filopodia and thin cell extensions that play major roles in migration, communication and cell adhesion. The filopodia secrete large amounts of proteolytic enzymes, which digest a path through the extracellular matrix (ECM). [32, 30, 31]

1.4 Delta-Notch Signalling

Delta-Notch signalling is a relevant route in the regulation of cell destination decisions. Certain chemical factors, such as VEGF, induce the expression of the delta-like 4 (Dll4) ligand by the ETCs, which leads to the activation of the Notch membrane receptors in the ESCs. The activation of this receptor attenuates their migratory behaviour. This Notch signalling pathway prevents an endothelial cell from adopting the ETC phenotype when one already exists in its vicinity. [30, 31]

2

Mathematical Introduction

2.1 Mathematical Model Classification

The mathematical model used in this project is conceptually based on the the model for angiogenesis developed in [30]. Angiogenesis models can be classified in three types, according to the form in which the cells and networks are presented: 1) continuous, 2) discrete and 3) hybrids.

Continuous models use a mesoscopic scale, an intermediate size scale between the macroscopic and the microscopic, and are regulated by partial differential equations. These models describe the network as a density of cells and base the flow of the chemicals on the principle of mass conservation. These considerations are usually based on the enzymatic biochemical reactions of Michaelis-Menten. [33]

Discrete models, however, use a microscopic description of the system, individually modelling cells with well defined spatial positions and treating them as units that move, grow and divide. These models have a large number of parameters which makes them difficult to adapt to larger systems. Still, this approach allows better comparisons with in vivo experiments. [34] A good example of a discrete model is the cellular potts model. This model is based on principles of statistical mechanics and can be seen applied to angiogenesis in [35]. The cells are placed in a network and are individually described as groups of points with a common identifier. The dynamics of the system is based on the process of minimization of a Hamiltonian, with the Monte Carlo and Metropolis-Hastings algorithms.

Finally, hybrid models use continuous aspects to describe the morphology of the networks and discrete aspects to describe some individual cells. Hybrid models are a good choice since they facilitate the description of the networks using a smaller number of parameter rules than discrete models. [34]

Table 2.1: Angiogenesis models Classification

Continuous Models	Discrete Models	Hybrid Models
- Mesoscopic scale; - Describe the network as a density of cells; - Partial differential equations; - The base of the flow of the chemicals is the principle of mass conservation (usually based on enzymatic biochemical reactions of Michaelis-Menten).	- Microscopic scale; - Cells modelled individually in well defined spatial positions; - Cells are treated as units that move, grow and divide; - Higher number of parameters; - Better comparisons with in vivo experiments.	- Uses continuous aspects to describe the morphology of the networks and the matrix; - Uses discrete aspects to describe the cells individually.

The model used in this project is a hybrid model. The discrete aspects of the system are used to describe tip cells, in the case of the blood vessel network, and tip of the growing TM, in the case of the glioblastoma network.

2.2 Phase Field Model

The continuous aspects of the model used in this project are based on the Phase Field methodology, which has received important contributions from the Landau's theory for phase transitions. [36]

When studying phase transitions of a thermodynamic system, it is common to analyse it on a microscopic scale using principles of statistical mechanics. When one arrives at an expression for the free energy of the system it is possible to obtain important information about the behaviour of the system, such as its entropy and specific heat. Depending on the aim of the study, it may also be interesting to analyse the existence of discontinuities in the free energy function, since a discontinuity corresponds to a phase transition. First-order phase transitions include solidification and condensation, which are characterized by the existence of latent heat and by the discontinuity in the first derivations of the free energy. Second-order phase transitions are continuous and do not involve the exchange of latent heat but second derivatives of the free energy are discontinuous. In cases where it is possible the analyse a complex system with a high number of particles at the microscopic level, this process is difficult and time-consuming. Thus, Landau's theory seeks to address this problem by presenting itself as a phenomenological theory which is able to ignore the microscopic aspects of the system. [36]

2.2.0.1 Order Parameter and Free Energy

In Landau's Theory of phase transitions, there is an important concept - the order parameter. This parameter is used to define and distinguish the domains in coexistence of phases of a given system. The order parameter can be represented by a scalar, vector or field tensor with different

values for different positions. Its definition depends on the purpose of the study. For example, in fluid-phase phase transitions, it is usually convenient to define the order parameter as a density ρ, in order to describe the state of the matter in a given region of the system. In the study of critical phenomena, the order parameter is defined in a way that makes it zero at the critical point. [3]

In Landau's Theory of phase transitions, the free energy F of the system can be written as a Taylor expansion series the order parameter ϕ, and it maintains the same symmetry properties of the Hamiltonian of the original system. Importantly, many systems with different microscopic behaviours end up being described by the same free energy function, as long as their Hamiltonians are invariant under the same transformations. A Hamiltonian is an operator that corresponds to the total energy of a system.

2.2.1 Phase Field Models in Phase Separation

In these situations, the phase field model introduces an order parameter that is a scalar field $\phi(\vec{r}, t)$. This order parameter is a function of position and time and assumes two values, representing the two states of the two coexistent phases in the system. A common example for this kind of order parameter is to take the value -1 in one of the system domains, 1 in the other domain, and the interface takes values close to zero. With this description there is no longer a need to define boundary conditions at the interface nor for its tracking. The use of this methodology in computational biology is now commonly used to address the study of important topics in biology such as multicellular systems, angiogenesis, and tumour growth.

Since the goal is to avoid boundary conditions at the interface, introducing a $\phi(\vec{r}, t)$ that varies smoothly and continuously, gives rise to a diffuse interface of a certain width ϵ. In fact, phase field models are also called diffuse interface models. A sharp interface is a particular case of a diffuse interface in which the width ϵ goes to zero, as can be seen in Figure 2.1.

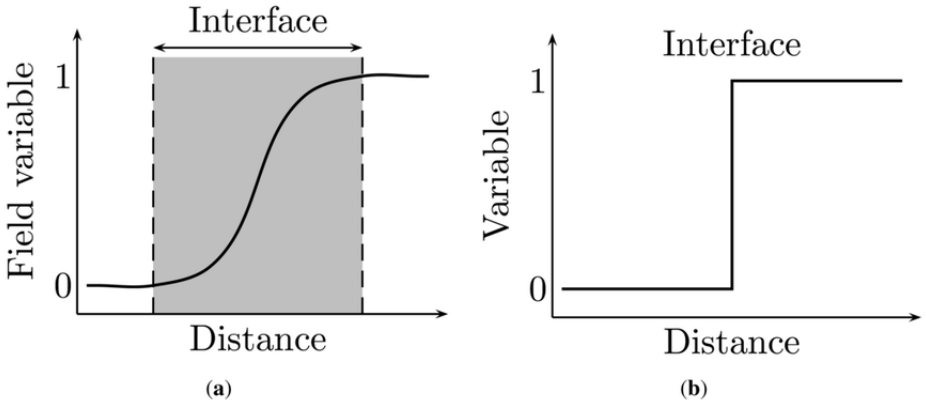

Figure 2.1: Graphs for the illustration of the difference between a diffusive (a) and a sharp (b) interface. [3]

In the phase field model, the order parameter $\phi(\vec{r}, t)$ does not need to have a meaningful interpretation since it can be just a form of identification for each domain. Since these models are interested in the study of the dynamics of the interface, the variations of behaviour at different

temperatures are ignored. It is assumed that the system is at sufficiently low temperature to allow the formation of the different domains.

2.2.2 Free Energy in the Phase Field Model: Functional $F(\phi(\vec{r},t))$

A functional is defined by a rule, which associates a number (real or complex) with a function of one or several variables, or, more generally, which associates a number with a set of functions. It is designated as a function of a function. The free energy functional of a phase field model, is written in a way that it depends on the order parameter $F(\phi(\vec{r},t))$ and contains all the information concerning not only the physical properties, but also the relevant interactions for the interface's dynamics.

$$F(\phi(\vec{r},t)) = \int (V(\phi) + \frac{\epsilon^2}{2}|\nabla\phi|^2)d\vec{r}$$

- $\nabla\phi$ represents the energy cost associated with of the interface, i.e. surface tension;
- ϵ represents the width of the interface;
- $V(\phi)$ is the potential characterized by two energy minimums that correspond to the two different states. This potential can be, for example, the double-well potential. (fig 2.2)

$$V(\phi) = -\frac{\phi^2}{2} + \frac{\phi^4}{4}$$

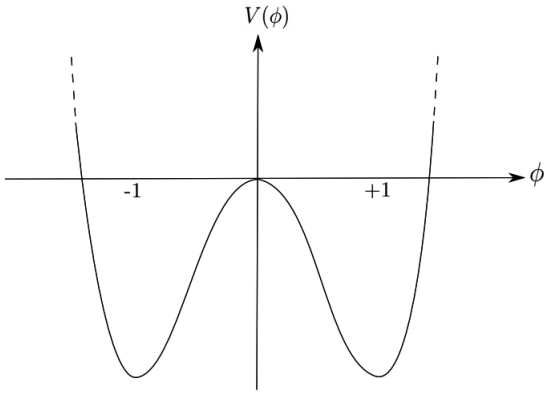

Figure 2.2: Double-well Potential $V(\phi)$ [4]

An easy example for the use of the double-well potential is when modelling tumour and non-tumour cells. In this case, $\phi = +1$ can be correspond to normal cells and $\phi = -1$ to tumour cells, ou vice-versa. If the the value of the potential were to be different in $V(\phi = +1)$ and $V(\phi = -1)$, the system would evolve to the less energetic state. Assuming that, for example, $\phi = +1$ refers to the tumour domain and corresponds to less energetic state, all normal cells would eventually be converted to tumour cells. If it corresponded to the higher energetic state, the tumour would disappear. However, using this approach to distinguish the two types of cells, is not a good practice for describing tumours since their growth would not be controlled and it would only be due to the initial shape.

Since the aim is to minimize the energy, the evolution of ϕ must be the opposite from the one

given by the gradient of $\frac{\delta F}{\delta \phi}$. The phase field model can be classified differently depending if this evolution is accomplished with or without conservation of ϕ.

2.2.3 Phase Field Model Classification

When the the order parameter is conserved, one is adressing the *Model B* which gives rise to the dynamics given by the Cahn–Hilliard equation. However, in phase field methodology there is also a model *Model A* and a *Model C*. In *Model A*, the order parameter is not conserved and its dynamics is given by the Allen–Cahn equation.

In order to find the time evolution of the ϕ, using the *Model B* one has to start with the conservation equation.

$$\frac{\partial \phi}{\partial t} + \nabla \cdot \vec{J} = 0$$

- Using Fick's Law, $\vec{J}$ represents the current of ϕ that is driven by the free energy functional of the system.

$$\vec{J} = -M \nabla \mu$$

- M is a mobility/diffusion coefficient that can either be a constant or a function;

- μ is the chemical potential of the system and it is defined as the functional derivative of the free energy functional F.

$$\mu = \frac{\delta F}{\delta \phi}$$

The Cahn–Hilliard equation is obtained by plugging the current $\vec{J}$ in the equation of the conservation of the order parameter.

$$\frac{\partial \phi}{\partial t} = \nabla \cdot (M \nabla \frac{\delta F}{\delta \phi})$$

This equation is the basis of *Model B*. It is a diffusion equation that can be simplified in the case when the coefficient M is not a function of ϕ, but rather a constant or a function of time.

$$\frac{\partial \phi}{\partial t} = M \nabla^2 \frac{\delta F}{\delta \phi}$$

The Allen–Cahn equation in which *Model A* is based, is obtained by assuming that the total quantity of ϕ can vary with time. In this way, the ϕ in a point may change independently in a way to locally minimize the energy.

$$\frac{\partial \phi}{\partial t} = -M \frac{\delta F}{\delta \phi}$$

Model C is used when one order parameter is not sufficient to describe the whole system and some extra coupled equations are needed. In this case other order parameters are added, each with their own dynamical equation.

Table 2.2: Phase Field Model Classification

Model A	Model B	Model C
- The total quantity of ϕ can vary with time; - Based on the Allen–Cahn equation: $\frac{\partial \phi}{\partial t} = -M\frac{\delta F}{\delta \phi}$;	- The order parameter is conserved; - Based on the Cahn–Hilliard equation: $\frac{\partial \phi}{\partial t} = \nabla \cdot (M\nabla\frac{\delta F}{\delta \phi})$; - If the coefficient M does not depend on ϕ, the equation can be simplified to: $\frac{\partial \phi}{\partial t} = M\nabla^2\frac{\delta F}{\delta \phi}$.	- Used when one order parameter is not sufficient to describe the system; - Other order parameters are added, each with their own dynamical equation.

In Interface Based Models the evolution of the interface can depend on elastic properties of the medium, surface tension, flow or chemical reactions. In order to introduce flow, a velocity field term such as $\nabla(\vec{v} \cdot \phi)$ can be added to the conservation equation. For a viscous system, one can use the Navier-Stokes equation and consider an external force proportional to $\phi\nabla(\frac{\delta F}{\delta \phi})$. When the model is focused on the interface there are less parameters to take into account because there is no need to describe every detail of the system. This makes it easier to determine the state of the domains and the integration. In order for these types of models to describe tumours one can add a proliferation term and a chemotactic term, as well as a coupled equation for the chemotactic factor.

3

Methods

3.1 Mathematical Model

The hybrid model used in this project, for both the modelling of the glioblastoma network and the blood vessel network, is based on the work developed by *Travasso et al.* [30]. The dynamics of the interface between the capillaries, the cells and the stroma is treated with a phase-field model formalism. In this project there is no interest in the criticality, but in the separation of phases far from the critical point, so we define the two order parameters as densities, not the difference. The activation of the tip cell phenotype in endothelial cells is implemented in the model through an agent-based component. The same approach is used for the tip of the TMs.

In the model there are introduced two effector factors. The blood vessels follow the gradient of an effective factor T^v that represents the balance between pro and anti-angiogenic factors. It is assumed that the cells release this factor until oxygen is properly delivered to them. The TMs that are created by the glioma cells follow the gradient of another effective factor T^g that represents the balance between the growth factors that are presumably involved in the process of the glioblastoma network formation. Both the cellular automata that represent the tip cell of the blood vessels and the ones that represent the tip of the TMs move with a velocity that is proportional to such gradient.

3.1.1 Equations and Assumptions

3.1.1.1 Effective Factors

$$\partial_t T^v = \nabla\cdot(D_v(r)\nabla T^v)\text{-}\alpha_{Tv} T^v \phi\Theta(\phi)$$
$$\partial_t T^g = \nabla\cdot(D_g(r)\nabla T^g)\text{-}\alpha_{Tg} T^g \psi\Theta(\psi)+\sigma(r)$$

- T^v is the effective factor for the blood vessel dynamics and is kept at constant value at the center of all cells;
- T^g is the effective factor for the tumour microtube dynamics of the glioblastoma cells;
- D_v is the diffusion constant for the T^v, the D_g is the diffusion constant for the D_g and are both assumed to be constant;
- Θ is the Heaviside function that takes the value 1 when its argument is positive and zero otherwise;

- α_{Tv} is the consumption rate of T^v and is calculated using the expression $\alpha_{Tv} = \frac{D_v}{R_v^2}$;
- α_{Tg} is the consumption rate of T^g and and is calculated using the expression $\alpha_{Tg} = \frac{D_g}{R_g^2}$;
- $\sigma(r)$ is the production rate for the T^g and it depends on the position since it is assumed that the production only occurs in the interface.

3.1.1.2 System Domains

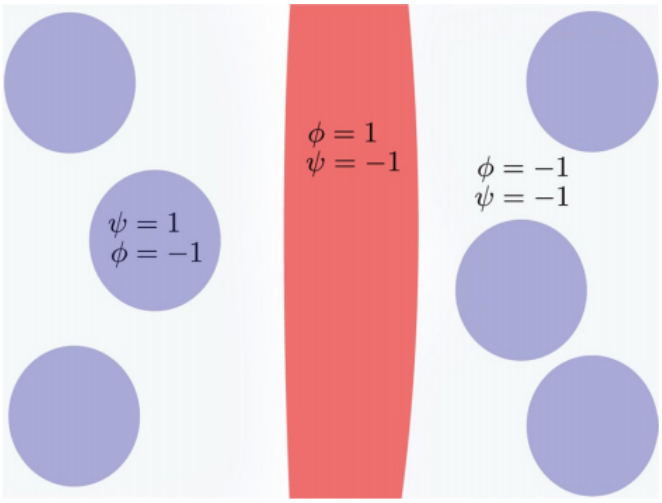

Figure 3.1: The value of the order parameters in different domains. The order parameter $\psi = +1$ inside the glioblastoma cells represented in blue and $\psi = -1$ outside, while the order parameter $\phi = +1$ inside the endothelial cells represented in red and $\phi = -1$ in the rest of the domain. The stroma is characterized by the region where ϕ and ψ are both negative. The model dynamics prevents the superposition between the positive domains of the two order parameters. [4]

$$\partial_t \phi = M_v \nabla^2 [-\phi + \phi^3 - \varepsilon \nabla^2 \phi + \gamma_v (\phi^2 - 1)(\psi^* - 2)(\psi^* + 1)^2] + \alpha_{Pv}(T)\phi\Theta(\phi)$$

$$\partial_t \psi = M_g \nabla^2 [-\psi + \psi^3 - \varepsilon \nabla^2 \psi]$$

- ϕ=1 and ψ=-1 represents a blood vessel.
- ϕ=-1 and ψ=-1 represents the stroma.
- ϕ=-1 and ψ=1 represents an individual tumour cell of a glioblastoma.
- M_v is the mobility coefficient for the endothelial cells of the blood vessels, M_g is the mobility coeficient for the glioblastoma, and both are assumed to be constant;
- α_{Pv} is the proliferation rate that is assumed to be constant;
- ϵ is the width of the interface;
- γ_v is the production rate and it is proportional to the energy cost and is set to have a high value in order to avoid an overlap in the simulations;
- ψ^* represents the local value of ψ at equilibrium state.

3.1.1.3 Network Movement

$$v_v = \chi_v \nabla T^v$$
$$v_g = \chi_g \nabla T^g$$

- v_v is the velocity of the chemotactically activated endothelial tip cell and v_g is the velocity of the chemotactically activated tip of the tumour microtubes;
- χ_v is the chemothatic response of the endothelial cells of the blood vessels to T_v, χ_g is the chemotactic response of the glioblastoma to T_g, and both are assumed to be constant;
- Endothelial tip cells are represented by agents with a constant radius R_v and the tip of the microtubes are represented by agents with a constant radius R_g.
- Due to Delta-Notch signaling, a new agent is introduced whenever there is a minimum effective factor located at a distance larger than four times the corresponding radius.

3.2 Computational Model

The simulations were performed with a discrete mesh with dimensions 300×300 with boundary conditions. The gradients and laplacians were calculated using a finite differences algorithm. The calculations for the new values of ϕ, ψ, VEGF and TGF, in each time step, were performed with Euler's method.

3.2.1 Finite Differences Algorithm

The partial differential equations used are linear in time and are diffusion-type equations. For this reason, the finite difference method is very useful. This method consists on the discretization of space, described by a parameter that gives the minimum distance between two points of the discrete space, which allows the evaluation of each functions in every point of the network. In this method, it is possible to improve the accuracy of the calculation of the space derivatives by adding more points to the discretization formula. [37] This was the method chosen for this work since it is quite simple to implement and it is simple to adapt changes in the model equations.

The Euler Method is well established and well known for the diffusion-type equations. [38] Though it is not fast and requires small time steps we gave more importance to the adaptability of the method to alterations in the model than its efficiency. Due to its simplicity to implement, this method was the chosen one.

3.2.2 *Initialize()*

In the code itself, the *initialize()* function sets the initial fields. In this function, the initial values of ϕ, ψ, TGF and VEGF are determined and the positions and dimensions of the cells and the initial blood vessel are defined.

It is also in this function that the order parameter $\psi(\vec{r}, t)$ is integrated in time before the simulation, in order to determine the interface between the glioblastoma cells and the stroma. Hence, the

simulation is performed with the glioblastoma cells fixed in space, since its only structural change intended with this model is the formation of the TMs.

In the model, the production of VEGF occurs at the center of glioblastoma cells. The production of TGF occurs only at the interface in order to create a gradient that promotes the movement of the cellular automata (CA) from inside to the outside of the cell .

3.2.3 *Step()*

The *step()* function deals with the temporal evolution of the system. For both dynamics (blood vessel network and glioblastoma network), the *boundx()* and *boundy()* functions deal with the boundary conditions of the system.

3.2.3.1 Blood Vessel Network Dynamics

Each cell of the system, if in hypoxia, produces VEGF. From the moment the cell is irrigated, that is, gets close to a capillary, VEGF is no longer produced inside the cell. To this end, in this function, there is a maximum radius for the search of a capillary in its vicinity, which determines whether this production of VEGF is switched off or not.

It is in this function that is performed the CA creation for the blood vessel network. This occurs only when the next four conditions are met:

1. The value of ϕ is greater than zero;
2. The value of ψ is less than zero;
3. The value of VEGF is greater than the cutoff defined;
4. The VEGF gradient is greater than the minimum VEGF defined.

The first and second conditions together allow us to make sure that we are inside a blood vessel.

Once these conditions are met, one has also to respect the rule of Delta-Notch signalling for the creation of the CA. This is achieved by determining the distances between the centres of the CA. This rule states that the creation of a new CA must be at a minimum distance of four radius from an existing one. In addition, it is also verified if the entire area of the CA to be created is completely inside the blood vessel. After the creation of the CAs, these are moved according to the VEGF gradient. In terms of movement, the function is written in such a way that the CAs, representing the endothelial tip cells, are not able to bypass the cells. In the case of the blood vessels this function also uses the auxiliary function *prol()* which is responsible for handling the proliferation mentioned in the previous chapter.

After the creation and movement of the CA, the new values of ϕ and VEGF are calculated, with the Euler's method, using the mathematical equations presented in the previous chapter. The new VEGF gradient is also calculated by this function.

3.2.3.2 Glioblastoma Network Dynamics

This function is also responsible for the CA creation from the inside of the glioblastoma cell. This occurs only when the next five conditions are met:

1. The value of ϕ is less than zero;
2. The value of ψ is greater than zero;
3. The type of the cell is zero which indicates that the cell has a TM producing phenotype;
4. The value of TGF is greater than the cutoff defined;
5. The TGF gradient is greater than the minimum VEGF gradient defined.

The first and second condition together allow us to make sure that we are inside a a glioblastoma tumour cell.

Once these conditions are met, just like in the case of the blood vessel network, a rule alike the Delta-Notch in vessels is imposed to guarantee a minimum distance between the TM tips. signalling for the creation of the CA is also taken into consideration. It is also made sure that the whole CA area is completely inside the cell. After the creation of the CAs, these are moved according to the TGF gradient. To explore several cases, more than one type of tissue cell was used. Some were able to produce the TMs and some were not, which gave raise to the third condition.

The new values of ψ and TGF are calculated, with the Euler's method, using the mathematical equations presented in the previous chapter. The new TGF gradient is also calculated in this function.

In the last part of this function, it is also taken into account the phenotype of the cell that is being taken into consideration. In the case of the two phenotypes (tumour and non-tumour cells), when a CA from a tumour cell reaches a non-tumour cell, the latter acquires a tumour phenotype, stops producing TGF and starts producing TMs. In the case of the three phenotypes, when a non-tumour cell is infected it acquires a new phenotype that stops producing TGF but is also not capable of producing TMs. In the case of only one phenotype this part os the function is ignored since there is no switch in phenotype when a CA reaches a cell.

3.2.4 *Out()*

The *out()* function is responsible for producing the output files, which are images such as the ones that can be found in the next chapter, and files for the values of the temporal evolution of the order parameters ϕ and ψ, and the values of VEGF and TGF.

3.3 Flowchart

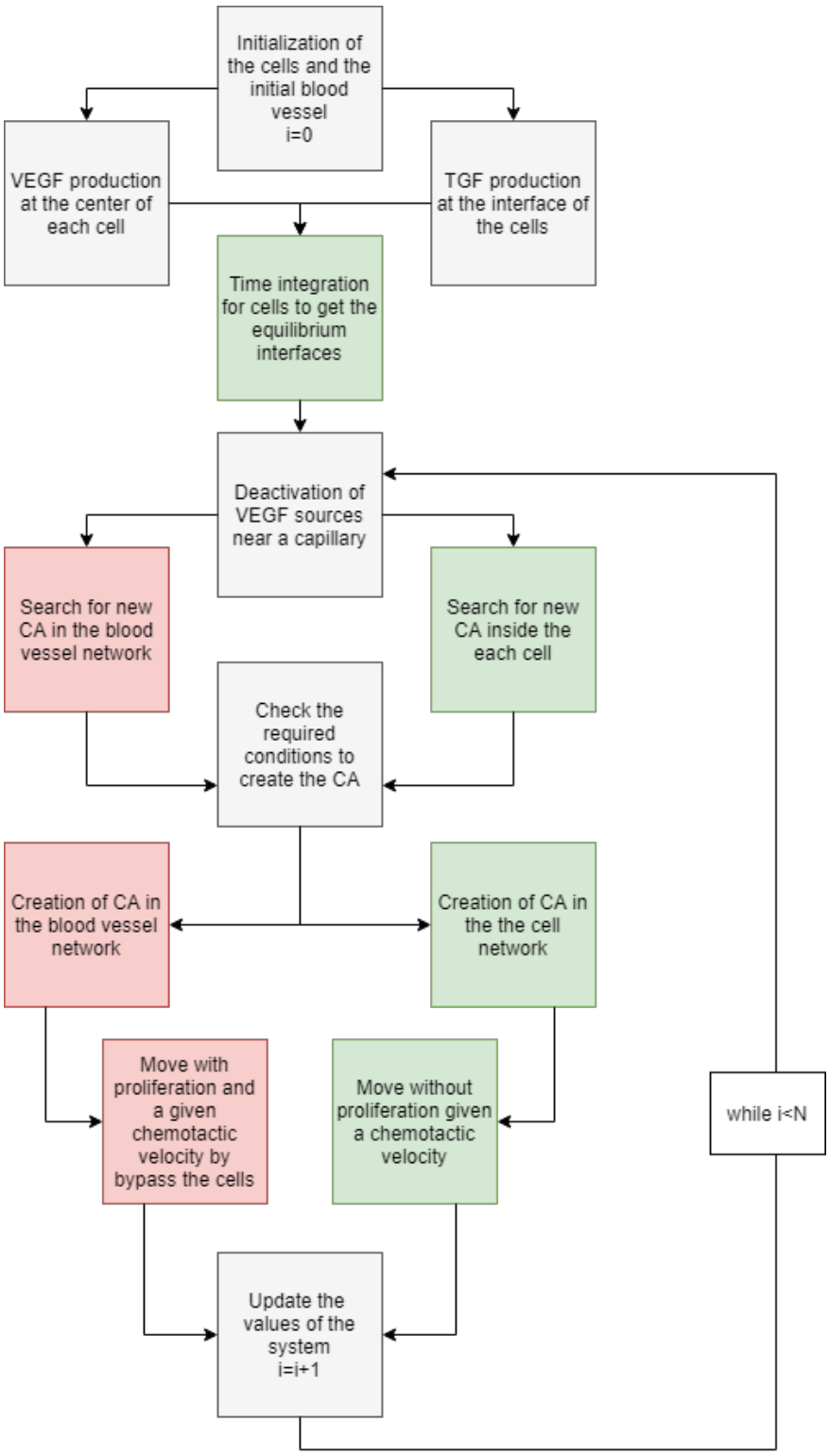

Figure 3.2: Illustrative flowchart to summarize the different types of steps to be followed in the program over time.

4

Results and Discussion

4.1 The influence of the number of Phenotypes regarding the production of TGF and TMs

In this chapter, the relevant results obtained with the model developed in this project and the respective analysis will be presented.

To illustrate the capabilities of this model, the first relevant results are some examples of the temporal evolution of the system, as well as the VEGF and TGF profile. VEGF is the effective factor T^v for the blood vessel network formation and TGF is the effective factor T^g that we assume to be responsible for the glioblastoma network formation. The time evolution for these two effective factors is determined by the equations presented in the last chapter.

- Phenotypes in terms of VEGF production:
  - V+ Cells are capable of producing VEGF;
  - V- Cells are unable to produce VEGF;
- Phenotypes in terms of TGF and TM production:
  - M+ Cells are capable of producing TMs but not TGF;
  - M- Cells are capable of producing TGF but not TMs;
  - M0 Cells are unable to produce TGF or TMs;
  - M1 Cells are able to produce both TGF and TMs;

The simulations were conducted with the value parameters presented in Table 4.1 and 4.2, in arbitrary units. These values were chosen while developing the code, based on the parameters presented in [4], with a few empirical alterations in order to achieve satisfactory qualitative results.

Table 4.1: Parameters related to the blood vessel dynamics, based on the ones presented in [4], with a few empirical alterations in order to achieve satisfactory qualitative results.

Parameter Description	Value
Initial width of the blood vessel	30
Radius of the endothelial tip cells (cellular automata) in the blood vessel network: R_v	6
Diffusion coefficient for VEGF: D_v	100
Mobility coefficient for the endothelial cells of the blood vessel network: M_v	1
Chemotactic response of the endothelial cells: χ_v	500
Proliferation rate of the endothelial cells: α_{Pv}	1
Maximum value for the concentration of VEGF for proliferation	0.3
Concentration of VEGF at the source	10
Minimum value of VEGF for branching	0.01
Minimum value for the VEFG gradient	0.01
Maximum velocity	0.03
Oxygen diffusion length	20

Table 4.2: Parameters related to the glioblastoma network dynamics, based on the the ones presented in [4], with a few empirical alterations in order to achieve satisfactory qualitative results.

Parameter Description	Value
Radius of the tumour cells	10
Radius of the tip of the tumour microtubes in the glioblastoma (cellular automata): R_g	4
Diffusion coefficient for TGF: D_g	100
Chemotactic response of the glioblastoma: χ_v	500
Rate of production of TGF: σ	5
Concentration of TGF ate the source	10
Minimum value of TGF for branching	0.1
Minimum value for the TGF gradient	0.005
Maximum velocity	0.03

The next simulations explore the mathematical model, studying the influence of the number of cell **phenotypes in terms of TGF and TM production**.

- **One Phenotype (all cells are M1)**: all the cells in the system are glioblastoma tumour cells and are all capable of producing both TGF and TM.
- **Two Phenotypes (cells are either M+ or M-)**: the cells in the system can either be non-tumour cells, capable of producing TGF, or glioblastoma tumour cells, capable of producing TM.
- **Three phenotypes (cells can be either M+, M- or M0)**: the cells in the system can either be non-tumour cells, capable of producing TGF, glioblastoma tumour cells capable of producing TM, or glioblastoma tumour cells incapable of producing TM.

It is important to understand that when we are studying only one phenotype M1 we are only

focused on understanding the formation of a cohesive and functional network and, on the other hand, when studying more that one phenotype, we are focused on the characterization of the networks and on the capacity for the tumour phenotype to propagate.

4.1.1 One phenotype

In the case of only one phenotype, the formation of the CA that corresponds the tip of TM is triggered by the TGF gradient inside each cell and its movement is driven by the TGF gradient produced by all tumour cells, which are also capable of producing TGF. When implementing this mechanism it made sense for the cells to only produce TGF along the interface and not at the center. This idea was carried out in order to create a gradient that could allow for the CA to move from the inside of each cell to the outside, instead of the opposite.

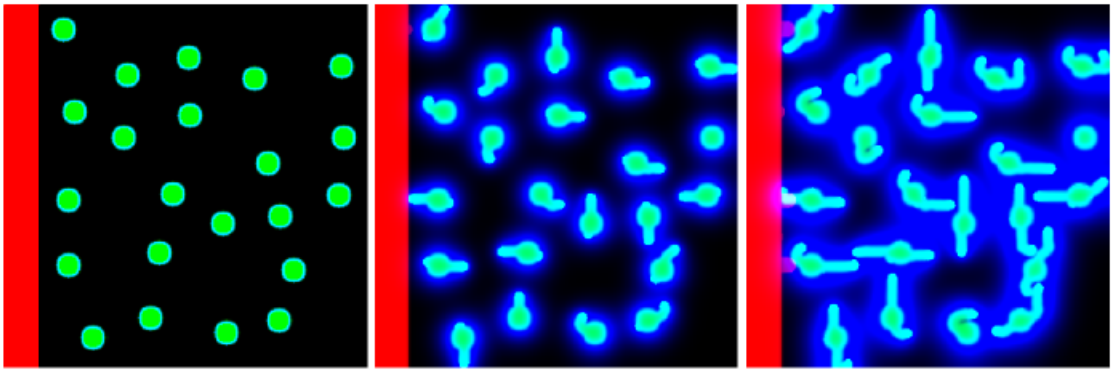

Figure 4.1: These images represent the temporal evolution of the system given by an initial condition with the glioma cells initialized at random positions. The three images represent the iterations at t=0; t=1000 and t=2000. In this case all cells are capable of producing TGF at the interface and are also all capable of producing TMs. The glioblastoma network is presented in green with a strong TGF production represented in blue. Since the aim of this approach is only to verify that this mechanism was not the appropriate one for describing the glioblastoma network formation, in order to achieve faster visual effects, the values of some of the constants for the network dynamics had to be raised higher than the values shown in Table 4.2. The diffusion coefficient was raised to 200, the concentration of TGF at the source was raised to 20 and the rate of TGF production was raised to 7. The main blood vessel is presented in red. The blood vessel sprouting phenomena appears only at iteration 2000, because the glioblastoma network formation peocess was speed up by the raise of the rate of TGF production. There is no interest in looking at this case any further since it is clear that this approach is unable to successfully create a cohesive network.

As expected, the cells were successfully capable of producing TM along the TGF gradient but were ultimately incapable of producing a network that connected the tumour cells, as one can see in figure 4.1. This can be easily explained since the driving factor that guides the movement of the TM is produced inside each cell. Therefore the gradient is higher near the cell which makes the TM go around in circles. For this same reason, in order for the CA to have a high enough gradient to be able to leave each cell, create a growing TM and achieve any visual results, the values some of the constants for the network dynamics had to be raised higher than the values shown in Table 4.2. The diffusion coefficient was raised to 200, the concentration of TGF at the source was raised to 20 and the rate of TGF production was raised to 7. Therefore, the TMs appear significantly

at iteration 2000, where blood vessels are only starting to be formed. However, the study of one phenotype serves merely to confirm that this approach is unable to successfully create a cohesive network. It seems that is therefore more probable that either there is a varied capacity between the tumour cells to produce TGF or that there is a more complex mechanism of guidance, for example, by the production of factors that bind TGF, better defining its gradient.

4.1.2 Two Phenotypes

In the case of two phenotypes, the formation of the CA that corresponds the tip of TM starts inside each glioblastoma tumour cell and is triggered and driven by the TGF gradient that is created by the TGF production in each non-tumour cell.

The results presented in Figure 4.2 correspond to the time-lapse of the system under the conditions described. The position of the each cell was chosen randomly. The first three images represent the temporal evolution at iteration number 2000, 4000 and 6000, respectively from left to right. The ones in the middle represent iteration number 8000, 10000 and 12000, respectively from left to right. The last three ones represent iteration number 14000, 16000 and 18000, respectively, also from left to right. The blood vessel network is shown in red and the tumour and non-tumour cells are shown in green. The non-tumour cells are the ones with with the blue interface, which indicates the TGF production. The glioblastoma tumour cells are the ones that do not produce TGF and, therefore, do not present the blue interface. Once a non tumour cell is linked to the network it becomes a tumour cell that is also capable of producing TMs.

As stated before, it is assumed that the production of this factor is what chemotactically attracts the formation of the tumour microtubes by the other cells. The glioblastoma tumour cells were successfully capable of producing the TM along the TGF gradient. This mechanism is ultimately capable of producing a large network, with only a few iterations, not only by connecting all the glioblastoma tumour cells but also by changing the phenotype of the majority of the non-tumour cells into tumour cells, in the system. Therefore, the mechanism for the two phenotype has been successfully implemented.

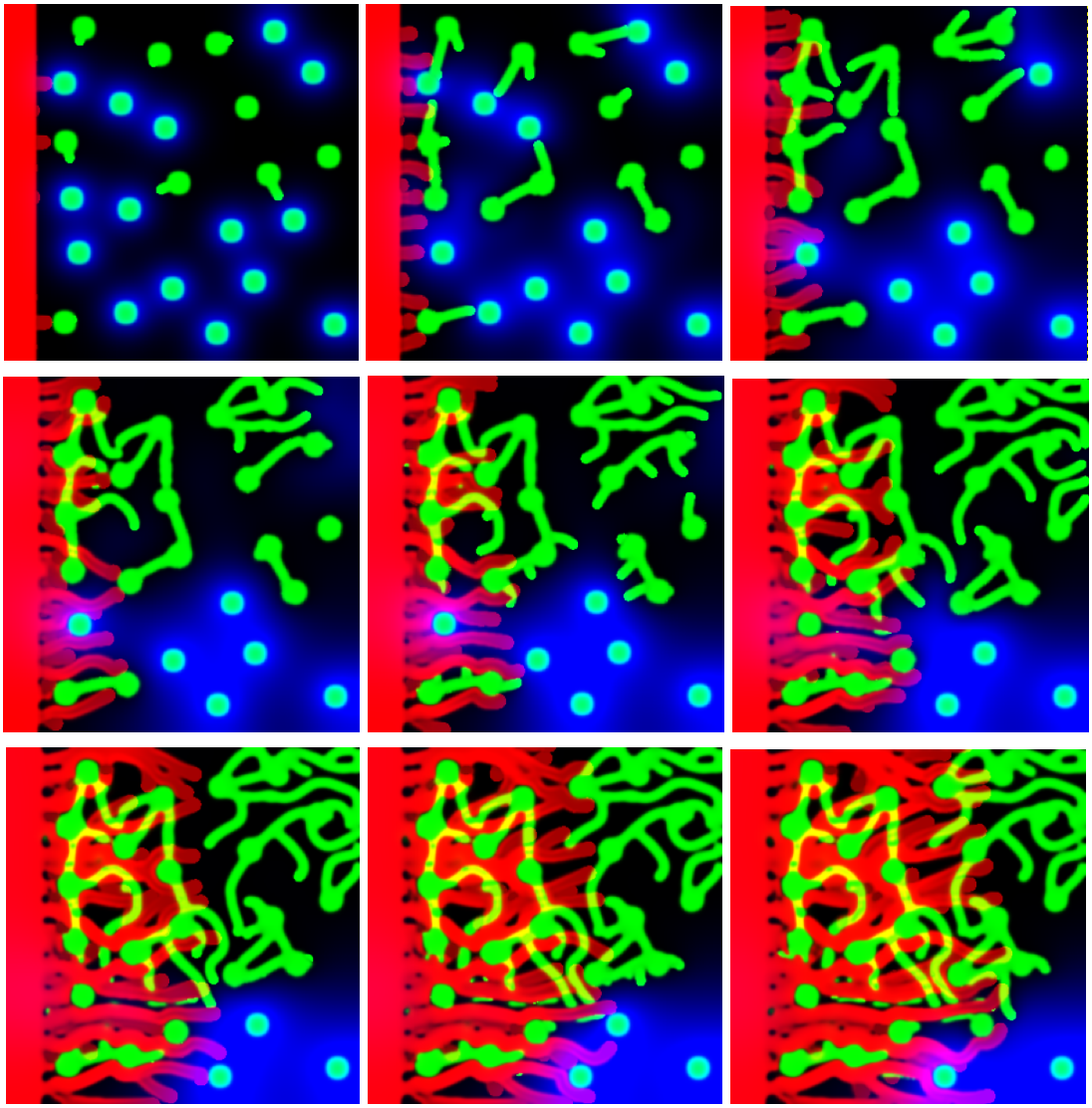

Figure 4.2: These images represent the temporal evolution given by a random initial condition. The three images on the top, represent the state of the system at iteration number 2000, 4000 and 6000, respectively from left to right. The ones in the middle represent the state of the system at iteration number 8000, 10000 and 12000, respectively from left to right. The ones below represent the state of the system at iteration number 14000, 16000 and 18000, respectively from left to right. In red there are shown the blood vessels and the glial cells are shown in green. The non-tumour cells are the ones with the TGF production. Therefore, they are the ones presented in green with the blue interface, since the TGF production occurs only on the interface. It is assumed that the production of this factor is what chemotactically attracts the formation of the tumour microtubes by the other cells. Hence, the glioblastoma tumour cells are the ones that do not produce TGF and do not present the blue interface.

In figure 4.3 it is presented the time-lapse evolution for the TGF levels across the system. As one can see, the first image on the left is the initial condition for the TGF and it is located only at the interface of the non-tumour cells. It is possible to see clearly in this example that this thin area of TGF production is not perfectly circular because of the algorithm used for the interpolation of the interface. This is the systematic error explained before that created the problem in the direction of growth of the TM when using only one phenotype. In the case of two phenotypes this systematic

error has no relevance since the cells that produce the TGF are not the ones that produce the CA and with the temporal evolution, the diffusion-like properties of this system are capable of diluting this error. As time passes, one can also see the approaching of the TM to the non-tumour cells since these are capable of consuming the TGF produced. When one of these TM reaches one non-tumour cell, the cell changes its phenotype and stops producing TGF. Now, the cell becomes a part of the glioblastoma network and starts not only consuming TGF from the system, but also producing TM to alter the phenotype of the other non-tumour cells.

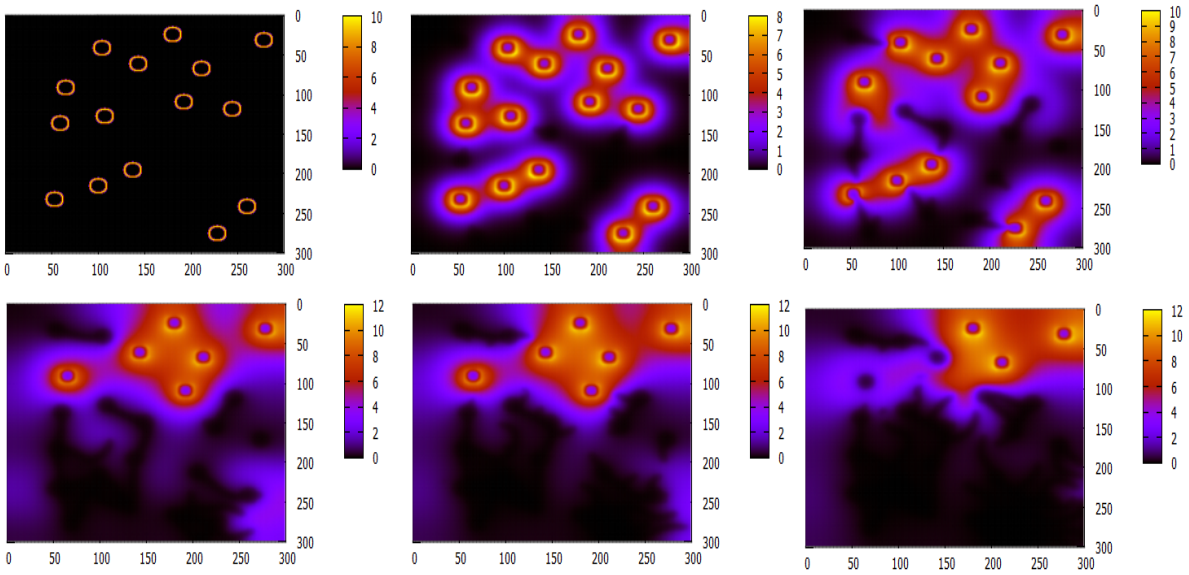

Figure 4.3: Time-lapse of the TGF evolution in the case of the two phenotypes. TGF is produced only at the interface of the non-tumour cells with the inital value of 10. Once the phenotype of a non-tumour cell is altered by a TM it stops producing TGF and starts consuming it.

In figure 4.4 it is presented the time-lapse evolution for the VEGF levels across the system. The first image on the left is the initial condition for the VEGF and, as one can see, this factor is produced at the centre of every cell, regardless of its phenotype. As time passes, once a capillary approaches a cell, the latter is no longer in hypoxia since it becomes irrigated. Therefore the production of VEGF is interrupted, as can be seen by the gradual disappearance of some of the VEGF peaks in the system.

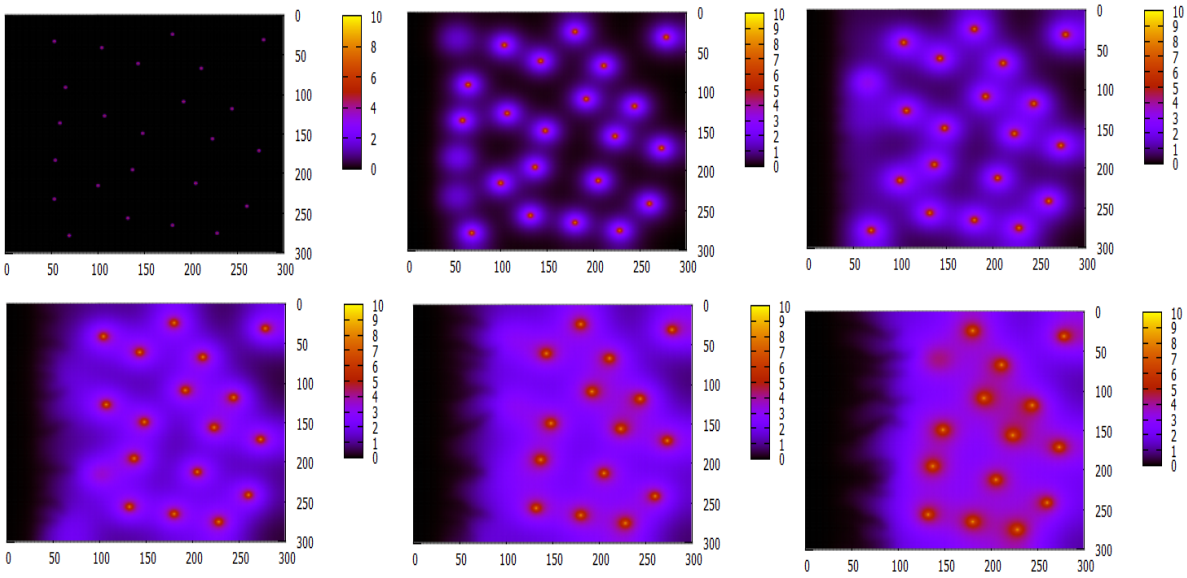

Figure 4.4: Time lapse of the VEGF evolution in the case of the two phenotypes. VEGF is produced at the centre of every cell with the initial value of 10. Once a cell is irrigated it stops producing VEGF.

4.1.3 Three cell phenotypes

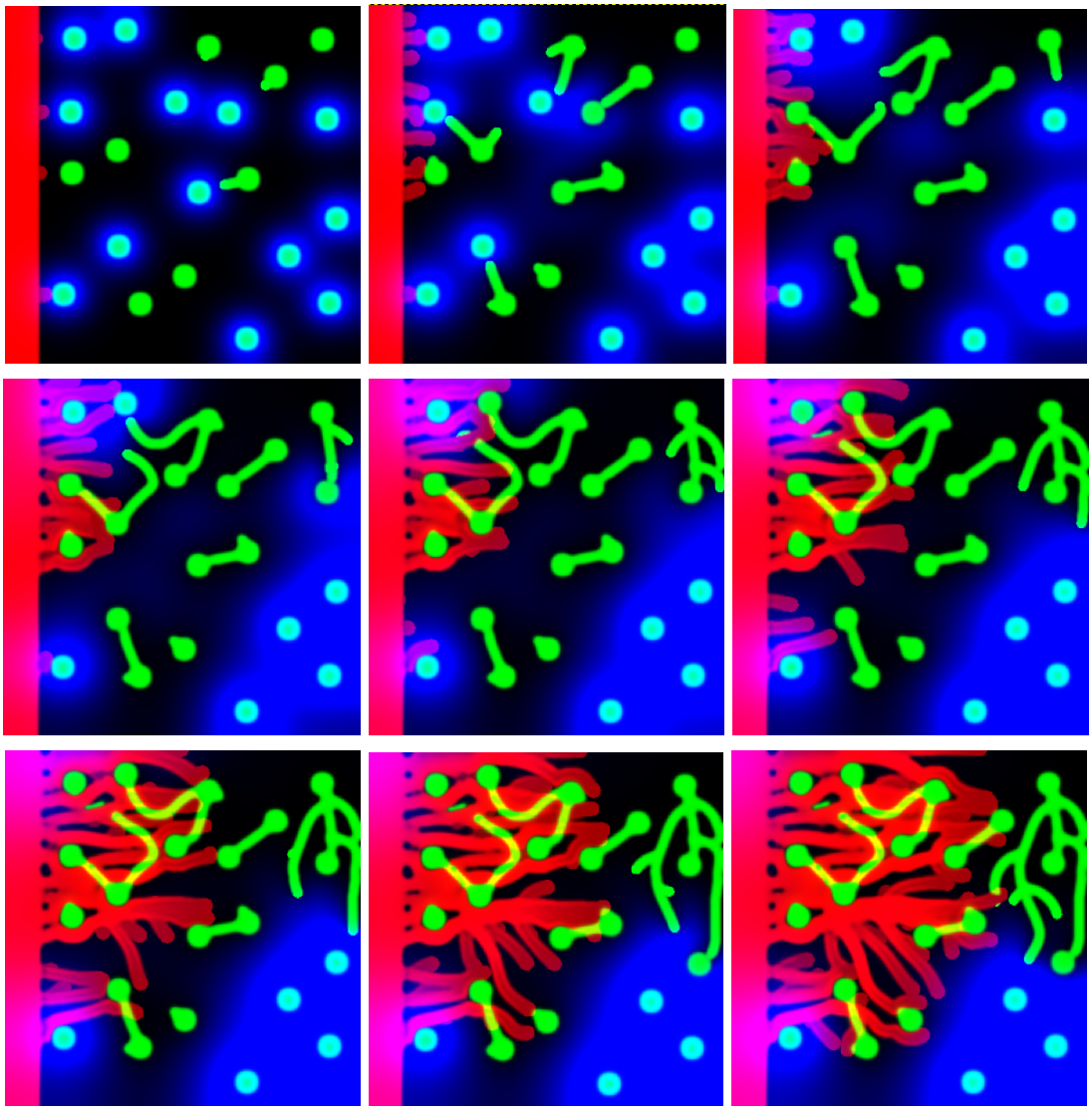

Figure 4.5: These images represent the temporal evolution given by a random initial condition. The three images on the top, represent the state of the system at iteration number 2000, 4000 and 6000, respectively from left to right. The ones in the middle represent the state of the system at iteration number 8000, 10000 and 12000, respectively from left to right. The ones below represent the state of the system at iteration number 14000, 16000 and 18000, respectively from left to right. The colour scheme used is the same as in image 4.2.

In the case of three phenotypes, the formation of the CA that corresponds to the tip of TM, as stated in the last mechanism, also starts inside each glioblastoma tumour cell and is also triggered and driven by the TGF gradient that is created by the TGF production in each non-tumour cell. The production of TGF is what chemotactically attracts the formation of the TM by the other cells. Once a TM reaches a non-tumour cell, the latter changes its phenotype and stops producing TGF but remains incapable of producing TM. The glioblastoma tumour cells were successfully capable of producing the TM along the TGF gradient. This mechanism is ultimately capable of producing small separate networks. It is capable of changing the phenotype the majority of

the non-tumour cells in the system. Therefore, the mechanism for the three phenotype has been successfully implemented.

The results presented in Figure 4.5 correspond to the time-lapse of the system. The position of the each cell was chosen randomly. The time interval between each image and the colour scheme is the same as previously described in the last mechanism. The sprouting of smaller vessels from the initial blood vessel is visible. The vessels are capable of contouring the cells, whether they are tumour or non-tumour cells. It is also visible the diffusion of the TGF produced by the non-tumour cells and the formation of the tumour microtubes originating from the tumour cells. In this particular mechanism, it is also clear that when a tumour cell from the glioblastoma encounters a non-tumour cell, the latter becomes acquires a new phenotype that stops producing TGF. However, as intended, this newly formed tumour cell is not capable of producing TM. The fact that the glial cells become tumour cells within the glioblastoma cluster but are incapable of producing more connections, results that this mechanism stops early on in the simulation. The blood vessels continue to grow in further iterations but the connections between the cells remain unchanged.

The existence of more than two phenotypes instead of the binary scenario of only tumour and non-tumour cells could be the reason behind the fact that some tumours are more confined and less invasive than others. There seems to be a possibility that some tumours can change the phenotype of non-tumour cells and turn these cells into new TM producing cells, whereas other tumours can change their phenotype but are not capable of turning them into TM producing cells.

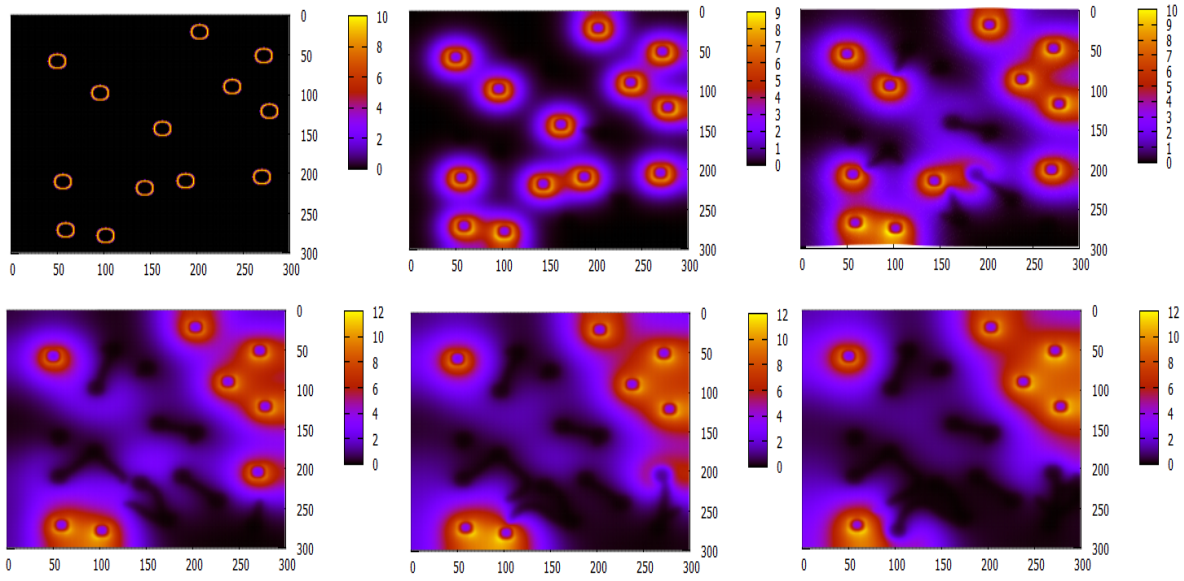

Figure 4.6: Time-lapse of the TGF evolution in the case of the three phenotypes. TGF is produced only at the interface of the non-tumour cells with the inital value of 10. Once a TM reaches a non-tumour cell it stops producing TGF and starts consuming it.

In figure 4.6 it is presented the time-lapse evolution for the TGF levels across the system. The first image on the left is the initial condition for the TGF and it is located only at the interface of the non-tumour cells. As time passes, one can see the approaching of the TM to the non-tumour cells since these are capable of consuming the TGF produced. When one of these TM reaches

one non-tumour cell, the cell changes its phenotype and stops producing TGF and starts not only consuming it.

In figure 4.4 it is presented the time-lapse evolution for the VEGF levels across the system. As one can see, the aspect of this evolution is the same as in the two phenotypes mechanism previously described.

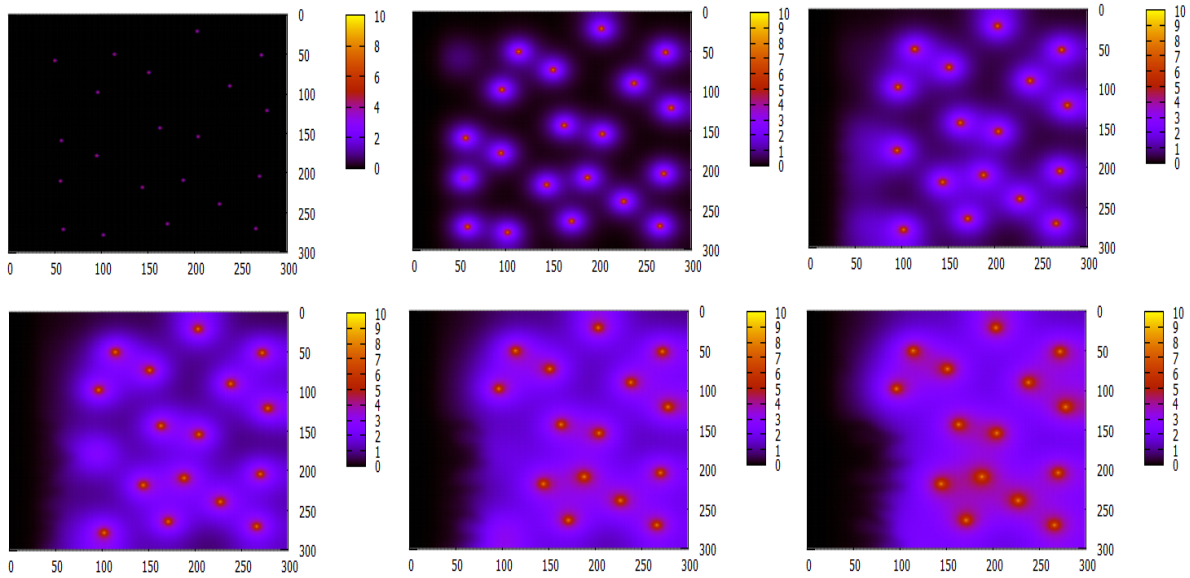

Figure 4.7: Time-lapse of the VEGF evolution in the case of the three phenotypes. VEGF is produced at the center of every cell with the inital value of 10. Once a cell is irrigated it stops producing VEGF.

4.2 Variation of TGF production

The mechanism that better produced a glioblastoma network similar to the ones that can be identified in the experimental images presented in the first chapter is the one that considers two phenotypes. It is easily relatable to the experimental results obtained for the astrocytoma, the most invasive type of glioma. Therefore, we will explore varying TGF production for this is the mechanisms expected, the cells were successfully capable of producing TM along the TGF gradient but were ultimately incapable of producing a network that connected the tumour cells, as one can see in figure 4.1. This can be easily explained since the driving factor that guides the movement of the TM is produced inside each cell. Therefore the gradient is higher near the cell which makes the TM go around in circles. For this same reason, in order for the CA to have a high enough gradient to be able to leave each cell, create a growing TM and achieve any visual results, the values some of the constants for the network dynamics had to be raised higher than the values shown in Table 4.2. The diffusion coefficient was raised to 200, the concentration of TGF at the source was raised to 20 and the rate of TGF production was raised to 7. Therefore, the TMs appear significantly at iteration 2000, where blood vessels are only starting to be formed. However, the study of one phenotype serves merely to confirm that this approach is unable to successfully create a cohesive network. It seems that is therefore more probable that either there is a varied capacity between

the tumour cells to produce TGF or that there is a more complex mechanism of guidance, for example, by the production of factors that bind TGF, better defining its gradient.

Figures 4.8, 7.9 and 4.10 represent a time-lapse of the evolution of the system will be presented given three values of the TGF production rate σ: 2.5, 5 and 7.5, respectively.

One can see that, with the first value (σ =2.5), at iteration number 10000, the glioblastoma network is the less well developed network and the less robust of the three. On the other end, the last value (σ =7.5) allows us to obtain a larger number of TMs for the same number of iterations. This indicates that this parameter determines the velocity of TMs creation. The number of connections for σ =5 is intermediate between the other two scenarios.

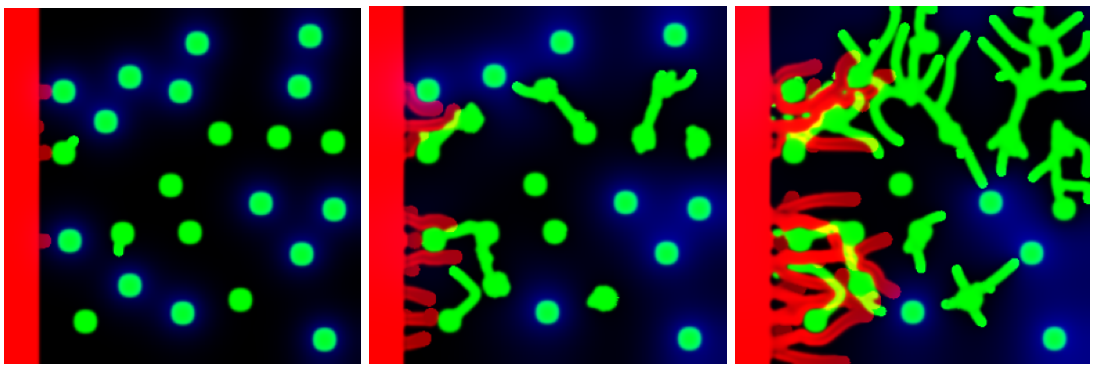

Figure 4.8: Time lapse example of the system's evolution with σ = 2.5 at t=2000; t=6000 and t=10000

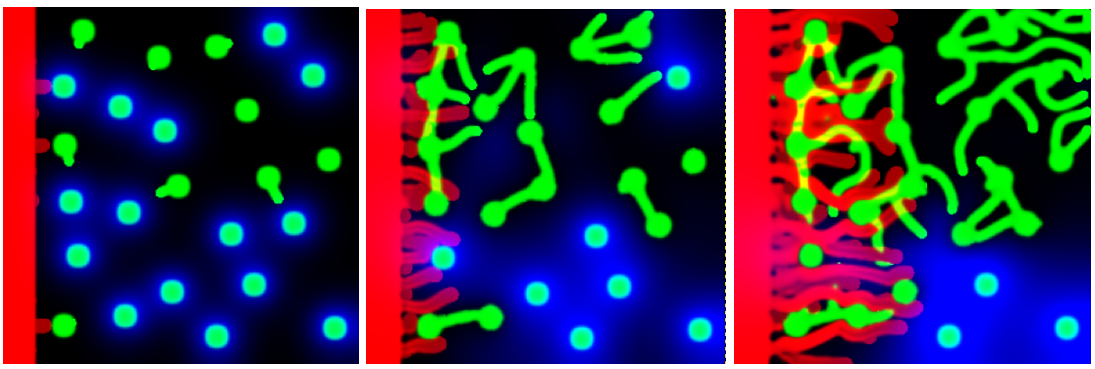

Figure 4.9: Time lapse example of the system's evolution with σ = 5 at t=2000; t=6000 and t=10000

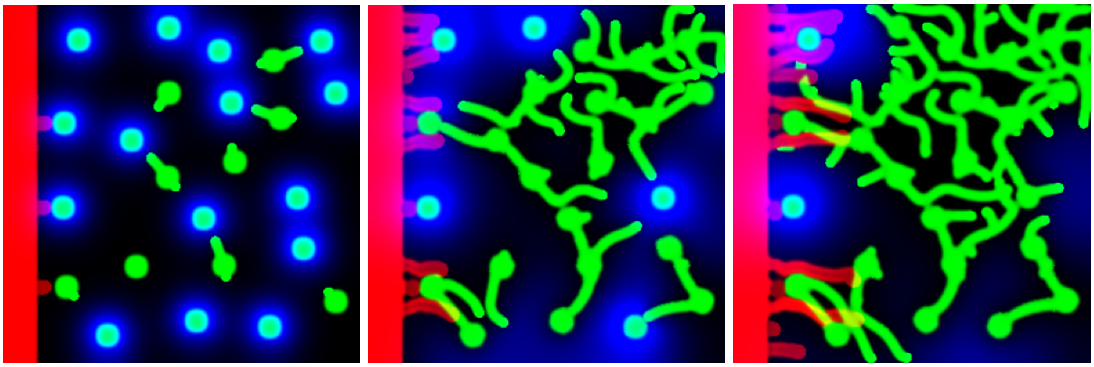

Figure 4.10: Time lapse example of the system's evolution with $\sigma = 7.5$ at t=2000; t=6000 and t=10000

4.3 Proportion of Non-tumour and Tumour Cells

In order to better understand the system and the influence of the parameter σ, an evaluation of the ratio of non-tumour and tumour cells was carried out. As the initial condition of both the number of tumour cells and non-tumour cells are chosen randomly, and for each σ value, three runs of the model with the two phenotype mechanism were performed and the mean value of the $\frac{C_N}{C_T}$ ratio was calculated over time.

4.3.1 Two phenotypes

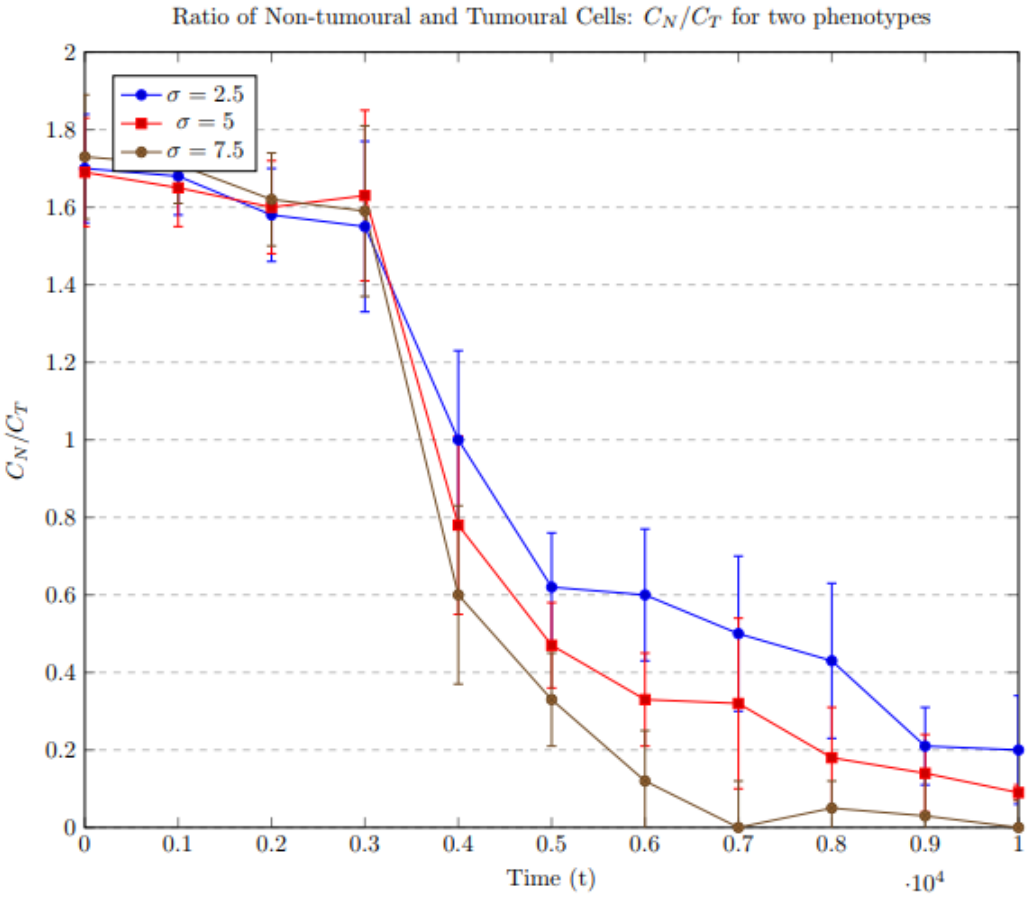

Figure 4.11: Time evolution of the proportion of Non-tumour and Tumour Cells $\frac{C_N}{C_T}$ given three values of the TGF production rate σ: 2.5, 5 and 7.5. The error bars represent the standard deviation based upon three simulation runs.

The value for $\frac{C_N}{C_T}$ remains constant for some time, until the TM of a tumour cell reaches a non-tumour cell. At a certain point in the simulation, here visible at iteration number 30000, this value drops dramatically since in this time, the TMs have typically the distance between 2 neighbouring cells. From the iteration 50000 forward, the ratio continues to decrease but more slowly since most of the cells were already with an altered phenotype. The ratio decrease is more pronounced the greater the value of σ, as previously shown.

4.3.2 Three phenotypes

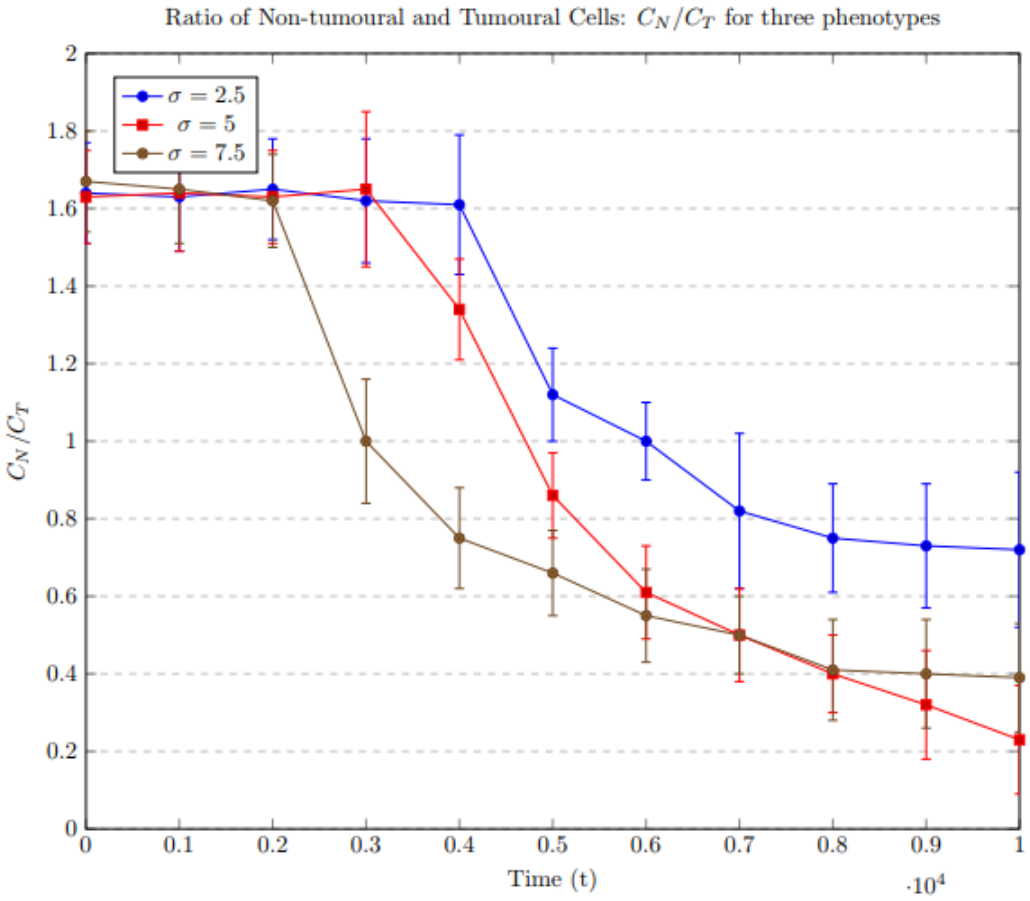

Figure 4.12: Time evolution of the proportion of Non-tumour and Tumour Cells $\frac{C_N}{C_T}$ given three values of the TGF production rate σ: 2.5, 5 and 7.5. The error bars represent the standard deviation based upon three simulation runs.

For the three phenotypes situation the value of $\frac{C_N}{C_T}$ also remains constant for some time, until a TM of a tumour cell reaches a non-tumour cell. At a certain point in the simulation, that is delayed by the decrease of σ, this value drops as time passes, but not as dramatically as in the case of the two phenotypes. The ratio stabilizes as the tumour cells cause the change in the others phenotype, because the latter do not acquire the same ability. In this case, the ratio decrease is also more pronounced the greater the value of σ.

4.4 Number of Connections between Tumour Cells

Additionally, also to better understand the system and the influence of σ, an evaluation of the number of connections between Tumour Cells was carried out.

4.4.1 Two phenotypes

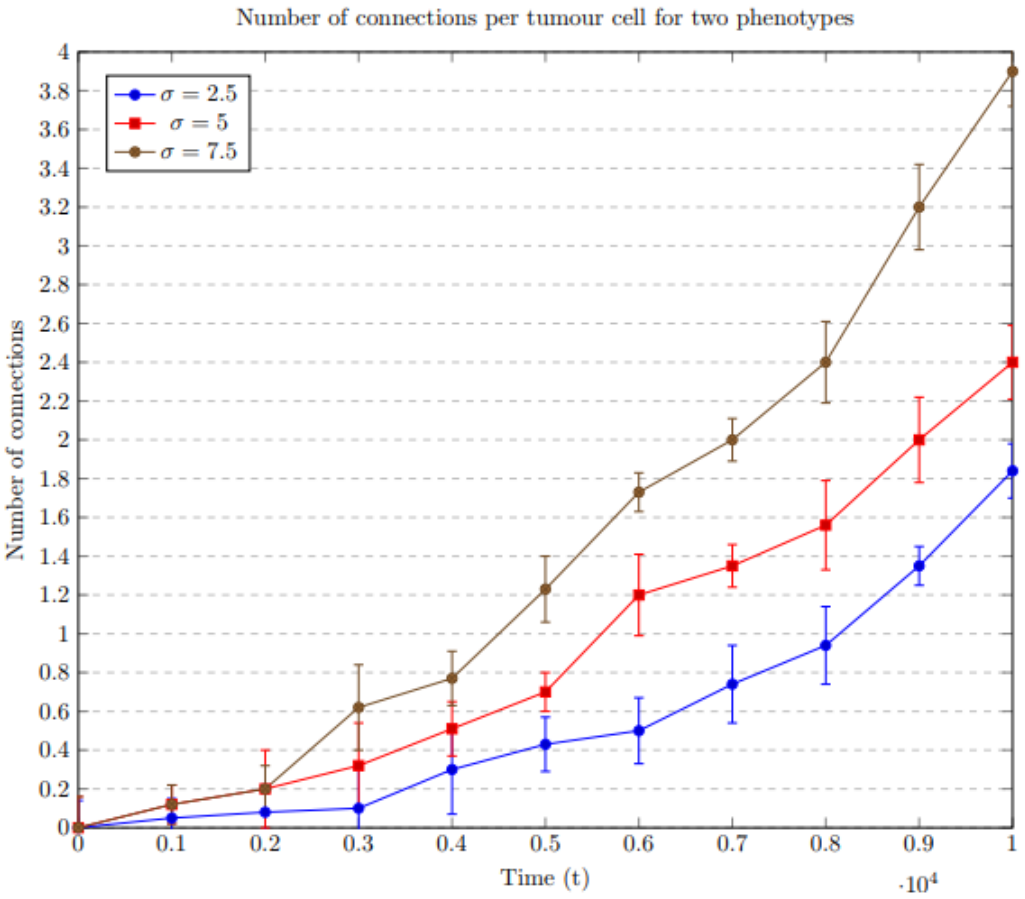

Figure 4.13: Time evolution of the number of Connections between Tumour Cells given three values of the TGF production rate σ: 2.5, 5 and 7.5. The error bars represent the standard deviation based upon three simulation runs.

It is important to note that the number of tumour cells increase as times passes, for this reason the sample for the mean value of the number of connections per tumour cell also increases with time as can be seen in Figure 4.13. In the same way as for the previous graphs, for each σ value, three runs of the model with the two phenotype mechanism were performed and the mean value of the number of connections per cell was calculated over time. For the case of the two phenotypes, the number of connections increases rapidly over time and the increase is faster the greater the value of σ.

4.4.2 Three phenotypes

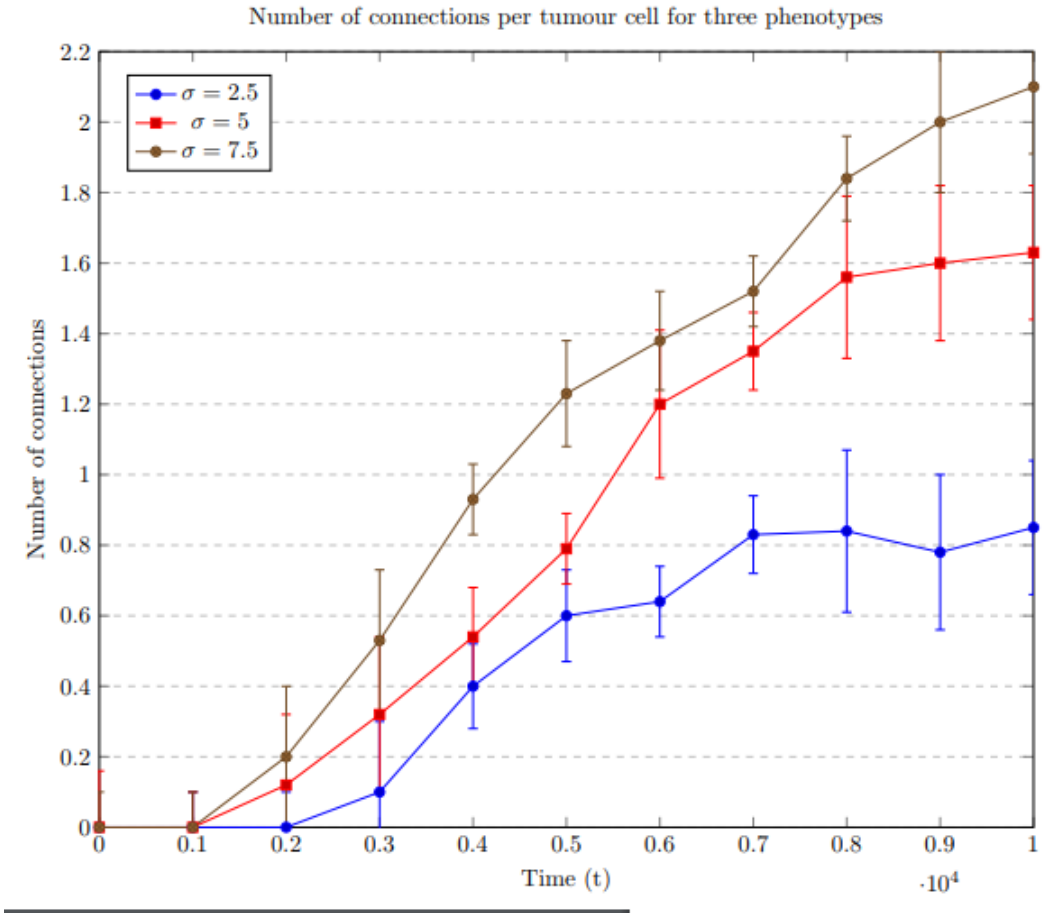

Figure 4.14: Time evolution of the number of Connections between Tumour Cells given three values of the TGF production rate σ: 2.5, 5 and 7.5. The error bars represent the standard deviation based upon three simulation runs.

In the case of the three phenotypes, the number of connections also increases over time but achieves lower values in comparison with the two phenotypes case. It starts with a fast pace and when it reaches iteration 6000 the number of connections starts to stabilize. This is exactly what would be expected since the cells with the altered phenotype are not capable of producing TMs. In the same way, the increase is more rapid the greater the value of σ.

4.5 Interaction between the Blood Vessel Network and the Glioblastoma Network

The way the model is implemented so far demonstrates two networks, a tumour and a blood that grow and evolve but do not have relevant interaction with each other. There is only one point of interaction between the two networks which is based on the fact that hypoxia cells are able to produce VEGF, promote the agiogenic process, and fail to produce VEGF when irrigated. Thus,

it is only the tumour network that is conditioning the evolution of the blood network and not the inverse. What is wanted is that both networks are able to interact with each other in order to study the impact of this interaction. The challenge is not then to understand how the tumour network affects the growth of vessels, but rather to understand how the growth of blood vessels can affect the growth and evolution of the network.

The hypothesis proposed is that the blood vessel network can have influence in the phenotype of each tumour cell. As already mentioned, the cells can be of two types with respect to the production of VEGF, they either produce or do not produce. With respect to microtubes, the best results were obtained with the two phenotypes explored before so this is the approach used for the next simulations. Therefore, cells can produce tumour microtubes and do not TGF or they can produce TGF and not tumour microtubes.

- Phenotype in terms of VEGF production:
  - V+ Cells are capable of producing VEGF;
  - V- Cells are unable to produce VEGF;
- Phenotype in terms of TGF and TM production:
  - M+ Cells are capable of producing TMs but not TGF;
  - M- Cells are capable of producing TGF but not TMs;
  - M0 Cells are incapable of producing both TGF and TMs;

What we have now is that the transition from V+ to V- depends on the distance to the vessels: if the cell is far from the vessel it is V+, otherwise it is V-. So far, for the microtubes, part of the cells were M+ and other M- and this assignment was made randomly at cellular distribution in the initial condition. What allows us to illustrate the invasive capacity of the tumour is precisely the mechanism of phenotype change. When a tumour microtube of an M+ cell reaches an M- cell, this M- cell becomes M+, that is to say it is capable of producing tumour microtubes.

Therefore, the hypothesis proposed for the influence of the network of blood vessels in the glioblastoma network is that the M+ and M- phenotype depend on the distance to the vessel, that is, it is proposed that the degree of irrigation of each of the tumour cells is determinant in the its ability to produce TGF or tumour microtubes. Thus, a struggling cell must be able to produce TGF. This is concretely revealed in the existence of two cut-offs rather than just one, as previously used for the production or non-production of VEGF. These two cut-offs will be designated Ra and Rb.

Just as before, to simulate the process of tumour invasion, whenever a TM of an M + cell encounters another M- cell, it transforms it into M +. The additional rules for this hypothesis are as follows:

Rule 1: Cells at a distance less than Ra from a vessel are V- and M+, meaning that they have enough energy to produce TMs but do not produce VEGF since they are irrigated;

Rule 2: Cells at a distance between Ra and Rb from a vessel produce VEGF but do not have enough energy to produce TMs, meaning they are V+ and can either be M0 or M- depending on the number of phenotypes (in the case of the two phenotypes they are M- and in the case of three phenotypes they are M0).

Rule 3: Cells at a distance greater than Rb produce TGFs but do not produce TMs. They are V+ and M-.

The only difference is the definition of the state of glioblastoma cells, which is then made as a function of distance from the vessel and not randomly. The dynamics of VEGF remain unchanged and the definition of TGF production is made in a similar way to VEGF in all iterations.

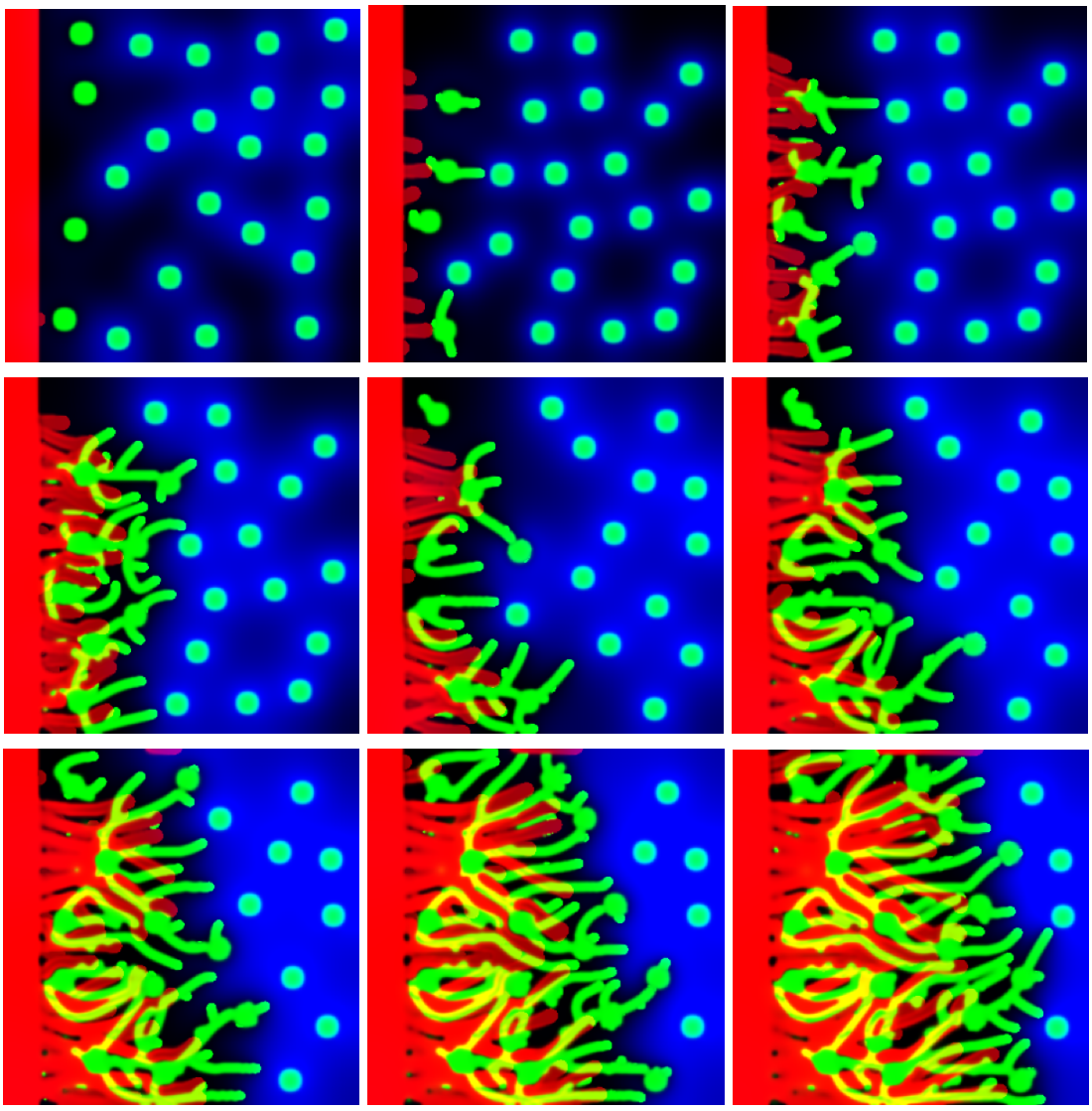

Figure 4.15: Time lapse example of the system's evolution with $\sigma = 5$ at t=1000; t=3000; t=5000; t=7000;t=9000; t=11000; t=13000; t=15000 and t=17000.

The implementations of the rules for the phenotype changes according to the distances are working properly. This is visible in that only non-irrigated cells are capable of producing TGF and only irrigated cells are capable of producing TMs. Still, some problems had to be resolved, since there ware too many vessels and the vessels were not forming a tree-like structure. This is because the VEGF produced is too high comparatively to the TGF production that drives de TM formation.

For the reasons pointed out before, it is necessary to place the results with the parameters acceptable for the production of VEGF. In order to do this, the value for the VEGF production was

lowered from 10 to 2. Additionally, several tests were performed to make sure the VEGF and TGF were diffusing at the same speed.

5

Conclusions and Future Work

Given the obtained results it is possible to conclude that the model presented and described in this thesis is able to propose dome hypothesis related to the formation of networks that are seen in the experimental results presented in the biological introduction.

Glioblastoma have different capacities for invading other tissues and changing their phenotype. The difference can be related to the capacity for the glioblastoma cells to produce TMs since it is seen that the greater the number of cells capable of producing TMs, the larger the network and the greater the invasion pattern. The support given by the blood vessels allows for the glioblastoma to perform this task.

Still, the creation of this model is just the beginning. Probably the most difficult improvement to implement, but also the most realistic would be to adapt the model to three dimensions. In this way it would also be possible to verify if the type of influence is presumed in this work that both networks impose in one another is enough to recreate what really happens *in vivo*. The system itself and the model is already complex and there are no experimental data that can give us a more detailed ideal about how in fact this tumour microtubes move.

Regarding the code developed to obtain the results, it could still undergo many improvements and optimizations in terms of speed and memory management. A more in-depth study with many more tests would also be needed to make sure that no bugs were left unnoticed. It would also be interesting to explore and use new tools and image programs in order to obtain better quality image results.

Bibliography

[1] J. Vinagre, A. Almeida, H. Pópulo, R. Batista, J. Lyra, V. Pinto, R. Coelho, R. Celestino, H. Prazeres, L. Lima, *et al.*, "Frequency of tert promoter mutations in human cancers," *Nature communications*, vol. 4, p. 2185, 2013.

[2] O. et al., "Brain tumour cells interconnect to a functional and resistant network," *Nature*, vol. 528, no. 7580, p. 93, 2015.

[3] N. Provatas and K. Elder, *Phase-field methods in materials science and engineering*. John Wiley & Sons, 2011.

[4] M. Moreira-Soares, R. Coimbra, L. Rebelo, J. Carvalho, and R. D. Travasso, "Angiogenic factors produced by hypoxic cells are a leading driver of anastomoses in sprouting angiogenesis–a computational study," *Scientific reports*, vol. 8, no. 1, p. 8726, 2018.

[5] J. R. Goodenberger ML, "Genetics of adult glioma. Cancer Genet.," vol. 205, p. 613–621, 2012.

[6] J. D. Mamelak AN, "Targeted Delivery of Antitumoral Therapy to Glioma and Other Malignancies with Synthetic Chlorotoxin (TM-601) Expert Opin Drug Deliv.," vol. 4, p. 175–86, 2017.

[7] T. Komori, "The 2016 who classification of tumours of the central nervous system: The major points of revision," *Neurologia medico-chirurgica*, vol. 57, no. 7, pp. 301–311, 2017.

[8] C. B. Johansson, S. Momma, D. L. Clarke, M. Risling, U. Lendahl, and J. Frisén, "Identification of a neural stem cell in the adult mammalian central nervous system," *Cell*, vol. 96, no. 1, pp. 25–34, 1999.

[9] N. Baumann and D. Pham-Dinh, "Biology of oligodendrocyte and myelin in the mammalian central nervous system," *Physiological reviews*, vol. 81, no. 2, pp. 871–927, 2001.

[10] V. A. Cuddapah, S. Robel, S. Watkins, and H. Sontheimer, "A neurocentric perspective on glioma invasion," *Nature Reviews Neuroscience*, vol. 15, no. 7, pp. 455–465, 2014.

[11] C. G. A. R. Network, "Comprehensive, integrative genomic analysis of diffuse lower-grade gliomas," *New England Journal of Medicine*, vol. 372, no. 26, pp. 2481–2498, 2015.

[12] J. E. Eckel-Passow, D. H. Lachance, A. M. Molinaro, K. M. Walsh, P. A. Decker, H. Sicotte, M. Pekmezci, T. Rice, M. L. Kosel, I. V. Smirnov, *et al.*, "Glioma groups based on 1p/19q, idh, and tert promoter mutations in tumors," *New England Journal of Medicine*, vol. 372, no. 26, pp. 2499–2508, 2015.

[13] B. Wiestler, D. Capper, M. Sill, D. T. Jones, V. Hovestadt, D. Sturm, C. Koelsche, A. Bertoni, L. Schweizer, A. Korshunov, *et al.*, "Integrated dna methylation and copy-number profiling identify three clinically and biologically relevant groups of anaplastic glioma," *Acta neuropathologica*, vol. 128, no. 4, pp. 561–571, 2014.

[14] F. A. Siebzehnrubl, D. J. Silver, B. Tugertimur, L. P. Deleyrolle, D. Siebzehnrubl, M. R. Sarkisian, K. G. Devers, A. T. Yachnis, M. D. Kupper, D. Neal, *et al.*, "The zeb1 pathway links glioblastoma initiation, invasion and chemoresistance," *EMBO molecular medicine*, vol. 5, no. 8, pp. 1196–1212, 2013.

[15] B. Wiestler, D. Capper, M. Sill, D. T. Jones, V. Hovestadt, D. Sturm, C. Koelsche, A. Bertoni, L. Schweizer, A. Korshunov, *et al.*, "Integrated dna methylation and copy-number profiling identify three clinically and biologically relevant groups of anaplastic glioma," *Acta neuropathologica*, vol. 128, no. 4, pp. 561–571, 2014.

[16] G. Cairncross, M. Wang, E. Shaw, R. Jenkins, D. Brachman, J. Buckner, K. Fink, L. Souhami, N. Laperriere, W. Curran, *et al.*, "Phase iii trial of chemoradiotherapy for anaplastic oligodendroglioma: long-term results of rtog 9402," *Journal of clinical oncology*, vol. 31, no. 3, p. 337, 2013.

[17] E. Lou, S. Fujisawa, A. Morozov, A. Barlas, Y. Romin, Y. Dogan, S. Gholami, A. L. Moreira, K. Manova-Todorova, and M. A. Moore, "Tunneling nanotubes provide a unique conduit for intercellular transfer of cellular contents in human malignant pleural mesothelioma," *PloS one*, vol. 7, no. 3, p. e33093, 2012.

[18] M. Inaba, M. Buszczak, and Y. M. Yamashita, "Nanotubes mediate niche–stem-cell signalling in the drosophila testis," *Nature*, vol. 523, no. 7560, p. 329, 2015.

[19] F.-A. Ramírez-Weber and T. B. Kornberg, "Cytonemes: cellular processes that project to the principal signaling center in drosophila imaginal discs," *Cell*, vol. 97, no. 5, pp. 599–607, 1999.

[20] S. Sowinski, C. Jolly, O. Berninghausen, M. A. Purbhoo, A. Chauveau, K. Köhler, S. Oddos, P. Eissmann, F. M. Brodsky, C. Hopkins, *et al.*, "Membrane nanotubes physically connect t cells over long distances presenting a novel route for hiv-1 transmission," *Nature cell biology*, vol. 10, no. 2, p. 211, 2008.

[21] I. F. Smith, J. Shuai, and I. Parker, "Active generation and propagation of ca2+ signals within tunneling membrane nanotubes," *Biophysical journal*, vol. 100, no. 8, pp. L37–L39, 2011.

[22] A. Rustom, R. Saffrich, I. Markovic, P. Walther, and H.-H. Gerdes, "Nanotubular highways for intercellular organelle transport," *Science*, vol. 303, no. 5660, pp. 1007–1010, 2004.

[23] K. V. Kuchibhotla, C. R. Lattarulo, B. T. Hyman, and B. J. Bacskai, "Synchronous hyperactivity and intercellular calcium waves in astrocytes in alzheimer mice," *Science*, vol. 323, no. 5918, pp. 1211–1215, 2009.

[24] A. H. Cornell-Bell, S. M. Finkbeiner, M. S. Cooper, and S. J. Smith, "Glutamate induces calcium waves in cultured astrocytes: long-range glial signaling," *Science*, vol. 247, no. 4941, pp. 470–473, 1990.

[25] L. Leybaert and M. J. Sanderson, "Intercellular ca2+ waves: mechanisms and function," *Physiological reviews*, vol. 92, no. 3, pp. 1359–1392, 2012.

[26] T. A. Weissman, P. A. Riquelme, L. Ivic, A. C. Flint, and A. R. Kriegstein, "Calcium waves propagate through radial glial cells and modulate proliferation in the developing neocortex," *Neuron*, vol. 43, no. 5, pp. 647–661, 2004.

[27] P. Carmeliet, "Angiogenesis in life, disease and medicine," *Nature*, vol. 438, no. 7070, p. 932, 2005.

[28] I. Buschmann and W. Schaper, "Arteriogenesis versus angiogenesis: two mechanisms of vessel growth," *Physiology*, vol. 14, no. 3, pp. 121–125, 1999.

[29] A. Köhn-Luque, W. De Back, J. Starruß, A. Mattiotti, A. Deutsch, J. M. Pérez-Pomares, and M. A. Herrero, "Early embryonic vascular patterning by matrix-mediated paracrine signalling: a mathematical model study," *PLoS One*, vol. 6, no. 9, p. e24175, 2011.

[30] R. D. Travasso, E. C. Poiré, M. Castro, J. C. Rodrguez-Manzaneque, and A. Hernández-Machado, "Tumor angiogenesis and vascular patterning: a mathematical model," *PloS one*, vol. 6, no. 5, p. e19989, 2011.

[31] T. H. Adair and J.-P. Montani, "Angiogenesis," in *Colloquium Series on Integrated Systems Physiology: From Molecule to Function*, vol. 2, pp. 1–84, Morgan & Claypool Life Sciences, 2010.

[32] M. M. D. S. Q. Guerra and R. D. Travasso, "Novel approach to vascular network modeling in 3d," in *2012 IEEE 2nd Portuguese meeting in bioengineering (ENBENG)*, pp. 1–6, IEEE, 2012.

[33] H. A. Levine, S. Pamuk, B. D. Sleeman, and M. Nilsen-Hamilton, "Mathematical modelling of tumour angiogenesis and the action of angiostatin as a protease inhibitor," *Computational and Mathematical Methods in Medicine*, vol. 4, no. 2, pp. 133–145, 2002.

[34] L. T. Edgar, S. C. Sibole, C. J. Underwood, J. E. Guilkey, and J. A. Weiss, "A computational model of in vitro angiogenesis based on extracellular matrix fibre orientation," *Computer methods in biomechanics and biomedical engineering*, vol. 16, no. 7, pp. 790–801, 2013.

[35] R. M. Merks, S. A. Newman, and J. A. Glazier, "Cell-oriented modeling of in vitro capillary development," in *International Conference on Cellular Automata*, pp. 425–434, Springer, 2004.

[36] F. F. Huang, *Engineering thermodynamics: Fundamentals and applications*. Macmillan College, 1988.

[37] K. W. Morton and D. F. Mayers, *Numerical solution of partial differential equations: an introduction*. Cambridge university press, 2005.

[38] J. Crank *et al.*, *The mathematics of diffusion*. Oxford university press, 1979.